Journal of Environmental Management 318 (2022) 115592

Contents lists available at ScienceDirect

Journal of Environmental Management

journal homepage: www.elsevier.com/locate/jenvman

A novel multi-model fusion framework diagnoses the complex variation characteristics of ecological indicators and quantitatively reveals their driving mechanism

Zijie Kong [a,b,1], Feifei Han [c,1], Hongbo Ling [d,e,f,*], Mingjiang Deng [a,g], Mengyi Li [a,b], Junjie Yan [h]

[a] State Key Laboratory of Hydraulic Engineering Simulation and Safety, Tianjin University, Tianjin 300192, China
[b] School of Civil Engineering, Tianjin University, Tianjin 300192, China
[c] College of Water Sciences, Beijing Normal University, Beijing 100875, PR China
[d] State Key Laboratory of Desert and Oasis Ecology, Xinjiang Institute of Ecology and Geography, Chinese Academy of Sciences (CAS), Urumqi 830000, China
[e] University of Chinese Academy of Sciences, Beijing 100000, China
[f] Xinjiang Aksu Oasis Agro-Ecosystem Observation and Experiment Station, China
[g] Xinjiang Ertix River Basin Development and Construction Management Bureau, Urumqi 830000, China
[h] Institute of Resources and Ecology, Yili Normal University, Yining 844500, China

ARTICLE INFO

Keywords:
Ecological indicators
Change patterns
Driving mechanism
Ecological restoration
Temporal trajectory
Sensitivity analysis

ABSTRACT

Systematic analysis of the change law and driving mechanism of ecological indicators (GPP, ET, WUE), as well as the study of maximum threshold of water resources benefit changing with ecological benefit, are important prerequisites for realizing the scientific allocation and efficient utilization of water resources in desert riparian forests. However, previous studies have defects in the detailed description of the change characteristics of ecological indicators. How to accurately diagnose the characteristics of a site, mutation year, pattern (linear, exponential, logarithmic, etc.), duration of change, future change trends of ecological indicators in a desert riparian environment, as well as quantitatively revealing their driving mechanisms, are major scientific problems that need to be solved urgently. In this regard, an ensemble function coupling a logistic function and an asymmetric Gaussian function was creatively adopted, a novel framework was created to integrate the time-series trajectory fitting method and the sensitivity analysis method, and the arid and ecologically fragile Tarim River Basin was taken as a typical area. The results showed that with enhanced water resource management in the Tarim River Basin, GPP, ET, and WUE all showed patterns of increasing change and could be expected to continue to rise or to remain at a high-level stable state. The longest continuous period of GPP change was 15 years, showing that ecological restoration is a long-term process. The years of GPP mutation were consistent with the implementation periods of major measures in the Tarim River Basin (1990, 2001, and 2011), indicating the reliability of this framework. More importantly, when GPP increased to 216.44 $g\,C\,m^{-2}$, the maximum WUE threshold of 0.93 $g\,C\,m^{-2}\,mm^{-1}$ occurred. This threshold can be used as a reference criterion for efficient utilization of ecological water in the basin. Among the ecological indicators studied, GPP was the most sensitive to environmental change, but GPP, with 80.60% of pixel area, showed a weak memory effect ($\alpha < 0.4$). Besides, GPP was the most sensitive to the leaf area index (LAI) and had the strongest correlation with it ($p < 0.001$). Therefore, LAI can be used as the main control factor for judging plant growth. This research can provide important scientific guidance and reference for the analysis of ecological indicator changes and the sustainable utilization of water resources in arid areas.

* Corresponding author. State Key Laboratory of Desert and Oasis Ecology, Xinjiang Institute of Ecology and Geography, Chinese Academy of Sciences (CAS), Urumqi 830000, China.
E-mail addresses: 18846921135@163.com (Z. Kong), hanfiefei2792@163.com (F. Han), linghongbo0929@163.com (H. Ling), xjdmj@163.com (M. Deng), 1724657017@qq.com (M. Li), yan3550@sina.com (J. Yan).
[1] These authors contributed equally to this study and share first authorship.

https://doi.org/10.1016/j.jenvman.2022.115592
Received 1 October 2021; Received in revised form 6 June 2022; Accepted 18 June 2022
Available online 25 June 2022

1. Introduction

The continuous increase in atmospheric carbon dioxide concentration will adversely affect global climate (Friedlingstein et al., 2020), but the vegetation of terrestrial ecosystems can slow down the rise of carbon dioxide concentration by providing a carbon sink (Piao et al., 2020). Dryland ecosystems cover ~41% of global land surface area (Yao et al., 2020), and desert riparian forest is their main component for carbon sequestration and water use. In addition, water resources are scarce in arid areas, and vegetation is sensitive to fluctuations in water supply, which controls the key regulatory factors of dryland ecosystems. Evapotranspiration (ET) and gross primary productivity (GPP) represent the total water vapor flux transported to the atmosphere by the ecosystem and the total amount of carbon dioxide fixed by photosynthesis. They are important components of the ecosystem water cycle and carbon cycle, respectively, and are also the key carbon and water regulation links in the ecosystem (Ryu et al., 2019; Tagesson et al., 2021; Jasechko et al., 2013). Water use efficiency (WUE) is the ratio of carbon gain (GPP) to water loss (ET), which is used to quantify the benefits of ecosystem water use (Keenan et al., 2013). Analyzing and studying the dynamic changes of ET, GPP and WUE in ecosystems and the driving mechanism of environmental factors behind them is of great significance for the protection of ecosystems in arid regions and the rational allocation of water resources.

Against the background of global change, different institutions and researchers have conducted extensive research on dynamic changes of GPP, ET, WUE in different surface ecosystems (Yao et al., 2020; Cheng et al., 2017). These studies clarified the basic information such as magnitude and direction of change in the three ecological indicators. However, under a series of artificial and natural disturbances such as climate fluctuation, afforestation and water resource regulation, actual experience with ecological indicators is a slow gradual change process (de Jong et al., 2012), which often includes the disturbance changes caused by external interference (Fang et al., 2018; Ma et al., 2019), whereas the perturbances of ecological indicators in long-term time series may not be found or may be completely concealed in the trend analysis. Detecting how and when ecological indicators change with sudden disturbances, can not only provide more insight into the change process of ecological indicators, but can also help people fully understand the response of ecological indicators to environmental change. In this regard, the first scientific question is proposed: how to accurately diagnose the response law that integrates the site, mutation year, pattern, duration, and past and future trends of desert riparian ecological indicators? In addition, in arid regions with limited water resources, carbon sequestration increases with more water supply (Poulter et al., 2014). However, a large amount of water input not only produces waterlogging stress on plants and inhibits biomass growth (Tagesson et al., 2021), but also greatly increases abiotic water consumption (i.e., evapotranspiration) (Liu et al., 2020), resulting in relatively low WUE. This indicates that there may not be a simple proportional relationship between WUE and GPP as water supply conditions change, but that there is a maximum threshold. Although some previous studies have investigated the relative contributions of GPP and ET to WUE change (Liu et al., 2020; Zhao et al., 2021), no research on the threshold relationship between WUE and GPP has been published up to now. In this regard, a scientific hypothesis was formulated: with increasing GPP, WUE reaches a maximum threshold.

The carbon-water cycle process in arid ecosystems is mainly driven by water availability (Ahlstrom et al., 2015). Precipitation is the water input of an ecosystem, which profoundly affect changes in ecological indicators (Fensholt et al., 2012). However, in arid ecosystems, rainfall is less than potential evapotranspiration, and surface runoff provides limited water supply to vegetation, so that groundwater (GW) resources are particularly important (Liu et al., 2017), but few studies have quantified the impact of GW on changes in ecological indicators. As for temperature, it provides the energy driving of photosynthesis, leaf transpiration, and soil evaporation (Yu et al., 2008). Studies have shown that temperature rise can advance the greening process of vegetation and delay dormancy, which directly affects the photosynthesis of vegetation and prolongs its growing season (Liu et al., 2020; Ryu et al., 2019). In the regulation of temperature on the physiological growth of vegetation, the saturated vapor pressure deficit (VPD), which is co-variant with temperature (Liu et al., 2020), can affect the magnitude of vegetation GPP and ET by regulating the stomatal conductance of leaves (Yuan et al., 2019). In addition to the direct impact of temperature and precipitation on the carbon-water cycle, they also lead to changes in vegetation structure (Chen et al., 2019), such as leaf area index (LAI), which in turn also change the carbon-water cycle, but the feedback of LAI on the carbon-water cycle has not been systematically studied. It can be seen that the carbon and water cycle processes of the ecosystem are not affected by a single factor, but by a combination of various factors. Furthermore, the combined or relative impact of various environmental factors has not been fully proved. Based on this, the second scientific question is proposed: how to quantitatively reveal the driving mechanism of changes in ecological indicators in a desert riparian environment? In addition, the disturbance of ecological indicators to environmental factors often has memory effects (The memory effect measures the ability of ecological indicators to return to a normal state after disturbance. The greater the memory effect, the stronger will be the anti-interference ability; in other words, the ecosystem can make timely adjustments to environmental changes) (Campos et al., 2013; Piao et al., 2020). Moreover, even when experiencing the same external disturbance, each part of an ecosystem community may respond differently due to differences in sensitivity (the degree of system change after disturbance) and elasticity (the ability of the ecosystem to restore its original state after disturbance) (Li et al., 2018). In view of this, it is urgent to deepen our understanding of the spatial distribution of areas with high sensitivity or low recovery rate, as well as the relevant ecosystem characteristics. An arid ecosystem is characterized as frail and highly sensitive. Therefore, the second scientific hypothesis is proposed: desert riparian GPP has weak memory effect and high sensitivity to environmental change.

For the gradual process of ecological indicators, a series of new algorithms such as the Detecting Breakpoints and Estimating Segments in Trend (DBEST) and Breaks For Additive Seasonal and Trend (BFAST) algorithms have been developed (Fang et al., 2018; Verbesselt et al., 2010),. However, this approach requires the user to set the number of breakpoints and use many mathematical models to fit the trajectory (Verbesselt et al., 2010), which makes the results highly uncertain and the calculation steps very complex. The time-series trajectory-fitting algorithm overcomes these shortcomings. It can not only detect the nonlinear change process of ecological indicators, but also determine the time and duration of ecological indicator change and predict future change. In addition, there is no need to set parameters manually, thereby reducing the deviation caused by subjective human factors. This method was first proposed by Zhang et al. (2003) and was used to detect vegetation phenology behavior in the northeastern United States. Moreover, the logistic model used in the algorithm can more effectively detect the gradual change process of vegetation under human disturbance, and has clear ecological significance (Song et al., 2016). However, it can only identify monotonic change processes of ecological indicators, but cannot identify non-monotonic change processes in which ecological indicators undergo degradation after restoration or the reverse. Che et al. (2014) solved this problem by adopting a new ensemble function: the non-monotonic change process could be detected by the Gaussian function form in the ensemble function. However, this function has not yet been used to analyze the detailed change characteristics of ecosystem GPP, ET, and WUE. Furthermore, it is also very important to reveal the driving processes that cause this change pattern. Based on autoregressive modeling, Seddon et al. (2016) proposed a new empirical method to determine the climate driving factors of vegetation productivity and regions with memory effects. This study used this

method to quantitatively analyze the driving mechanism of ecological indicator changes.

Based on the analysis just described, to solve two scientific problems and verify two scientific hypotheses, this study involved the building of a new type of multi-model fusion framework. With the aid of multi-source remote-sensing data and measured groundwater depth data, the complex variation characteristics of ecological indicators at pixel and reach scale were analyzed, the sensitivity of ecological indicators to a changing environment was studied, the driving mechanism of ecological indicator change patterns was revealed, the ecological regulation zone was delineated, and the maximum threshold point of WUE changing with GPP was determined. This study provides important guidance and scientific reference for promoting ecological restoration and efficient utilization of water resources in arid areas.

2. Materials and methods

2.1. Overview of the study area

The Tarim River Basin (34.20°–43.39°N, 71.39°–93.45°E, Fig. 1) has a typical continental arid climate. Annual rainfall is only 17.4–42.0 mm in the Tarim River Basin, whereas annual evaporation is as much as 2500–3000 mm (Ling et al., 2016). This basin is one of the most ecologically fragile regions in China and the world. The basin includes 144 tributaries of nine major rivers, which occupy an area of 1.02×10^6 km^2 (Ling et al., 2019). The Tarim River is the longest endorheic river, with a length of 1321 km (upstream from Alar to Yingbaza, midstream from Yingbaza to Qiala, and downstream from Qiala to Taitema Lake) (Ling et al., 2020). Currently, only the Aksu, Hetian, Yarkand, and Kaidu-Kongqi Rivers have surface water connections with the Tarim River; the rest of the river system has separated from the mainstream due to climate change, human activities, and other factors (Ling et al., 2016). Specifically, after completion of the Daxihaizi Reservoir in 1972, the flow from the upstream and midstream portions of the Tarim River was completely blocked, leading to the drying up of the downstream portion of the Tarim River and Taitema Lake, the large-scale degeneration of natural vegetation, groundwater recession, and serious damage to the ecological environment (Ling et al., 2019) (Fig. 1a). To save the ecosystem in the downstream area, in 1990, the Tarim River Basin Management Bureau was established to implement ecological protection and ecological water supply for the Tarim River. In 2001, the Chinese government invested 10.7 billion yuan to carry out comprehensive management of the Tarim River Basin with the fundamental aim of restoring the downstream ecosystem. To further guarantee an ecological water supply for the Tarim River, the four source streams were placed under uniform administration by the Tarim River Basin Management Bureau in 2011, so that water resource management was increasingly strengthened.

From 2000 to 2018, ecological water replenishment was carried out nineteen times in the downstream portion of the Tarim River, with a total ecological water replenishment of 7.767 billion m^3 and an average annual water replenishment of 432 million m^3. The ecological environmental degradation trend in the Tarim River Basin has been effectively curbed: groundwater depth in the basin has risen significantly, the flow now reaches Taitema Lake, the impacts of long-term flow cut-off in the downstream area are being mitigated, and green vegetation in the riparian zone shows positive physiological and ecological responses (Liu et al., 2013) (Fig. 1b and c). Therefore, the Tarim River Basin is not only the area with the most serious ecological degradation caused by artificial interference, but also a typical case of the most successful ecological restoration promoted by human intervention.

2.2. Datasets and pre-processing

GLASS, which is characterized by long time series, high spatial resolution and provide reliable data to study global environmental change. It is widely used in climate, hydrology, and disaster studies at global and regional scales (Jiang et al., 2017; Liu et al., 2018). The GLASS dataset is inverted by integration of many algorithms such as the Bayesian method and machine learning (Yao et al., 2015) based on multi-source remote sensing products and measured site data. The dataset contains 16 products with a maximum temporal and spatial resolution of 8 days and 500 m, respectively, covering the period 1981–2018. GLASS is published by the Center for Global Change Processing and Analysis of Beijing Normal University and is available for free download at http://www.geodata.cn/. It is widely used in research on global and regional change and has high reliability compared to similar remote-sensing products. Chu et al. (2011) found that GLASS LAI was superior to MODIS LAI (C4)

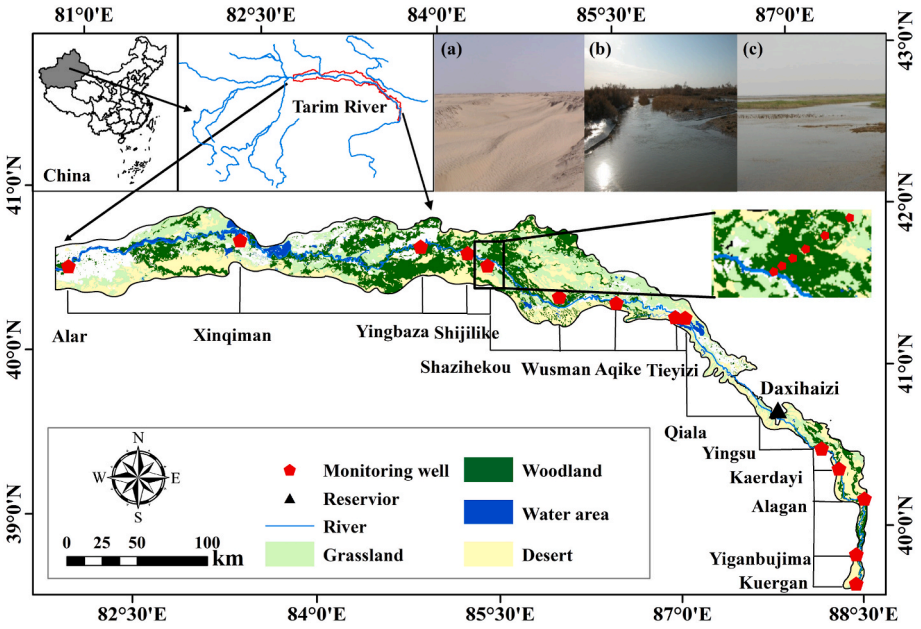

Fig. 1. Overview of the Tarim River Basin, including its land cover type, location in China, distribution of water system, location of groundwater monitoring wells, etc. (a), (b), and (c) represent the landscape changes of the terminal Taitema Lake during river cut-off, under and after ecological water delivery, respectively.

in simulating climate impact on large-scale vegetation restoration in Queensland, Australia. Quantitative comparisons of these time profiles indicate that GLASS has a smoother time profile, whereas the MODIS data curves show significant volatility, especially during the growing season (Xiao et al., 2016). In addition, the accuracy of GLASS is significantly higher than that of MODIS. Xiao et al. (2011) used MODIS surface reflectance data and measured LAI data from eight BELMANIP sites for validation. The results showed that, compared with MODIS LAI products, GLASS LAI products are relatively smooth, and their accuracy is significantly better. Based on these reasons, GLASS remote-sensing data products were selected in this study to analyze the long-term change rules of ecological indicators.

The GLASS datasets used in this paper are shown in Table S1. GPP and ET were used to analyze the spatial gradual change pattern of ecological indicators, and the 1 km × 1 km 8-day ET values were further upscaled to 500 m × 500 m using the nearest-neighbor resampling algorithm to match the spatial resolution of the gridded GPP dataset. In this study, water use efficiency (WUE) is defined as the amount of carbon sequestration per unit of water loss in an ecosystem (Keenan et al., 2013) and can be calculated by the ratio of GPP and ET. LAI data were used to analyze the driving mechanism of ecological factor change in desert riparian forest. To compare the change patterns of ecological indicators before and after ecological water diversion, GLASS GPP AVHRR (0.05°, 1982–2018) and GLASS ET AVHRR (0.05°, 1982–2018) data were also used. To ensure consistency, these data were preprocessed before analysis as follows: the Interactive Data Language (IDL) was used to read, splice, cut, and synthesize the growing season data (from April to October) from GLASS data and to perform format conversion, reprojection, and projection conversion.

Other datasets used in this article are shown in Table S1, including gravity satellite data, land surface models, and monitoring data. All remote-sensing and monitoring data were unified to growing-season scale and a spatial resolution of 500 m/0.25 °. Specifically, the VPD data were inverted from the LST data (Appendix, Methods S1). The groundwater depth data were inverted from the GRACE and GLDAS satellite datasets, and the measured groundwater depth data were used to adjust the inverted groundwater depth data (Appendix, Methods S2). The data were then used as model inputs to construct a multi-model fusion framework that combines (1) pattern recognition and (2) driving mechanism detection. The calculation program for the framework was written in R, and ArcGIS 10.6 and Python 3.7.8 were used to draw the results graph (the overall research process is shown in Fig. 2).

2.3. A novel multi-model fusion framework

The novel multi-model fusion framework constructed in this study includes two modules: (1) an integrated function, coupled with the logistic function and the asymmetric Gaussian function, was used to identify the change patterns, the location of breakpoints, and future change trends. (2) The ARI multiple regression analysis model helps to examine the relative importance of the driving factors, identify the memory effect and quantify the sensitivity of the ecological indicators by calculating the sensitivity index. Combined with the structural equation model (SEM), the driving mechanism of ecological indicator change can be revealed.

2.3.1. An integrated function to identify patterns of ecological indicator change

Using time series of remote-sensing data, several methods have been developed to obtain the law of gradual change of ecological indicators. However, these algorithms focused only on the monotonic change process of ecological indicators during the study period and did not address more complex change processes. Based on this, an integrated function coupled with a four-parameter logistic function and an asymmetric Gaussian function was used in this study to automatically identify the patterns of ecological indicator change, and then the direction, intensity, and time of ecological indicator change were determined to predict future change trends.

To eliminate the influence of periodic and irregular fluctuations in the time series, the original time series (series x) was first smoothed using the moving average method (setting the window length to 3) to obtain a more stable time series (series y). When ecological indicators are disturbed, they enter a state of rapid improvement or deterioration. It was assumed that the time point (P) with the maximum slope of the time-series profile of ecological indicators was the mutation year. In this study, the first-order derivative of the smoothed time series (series y) was calculated and P corresponded to the maximum value of the derivative represents the moment when the ecological indicators change fastest.

To better identify nonlinear change patterns, this study took P as the center point to extend the smoothed processed series y. The extended series k was filled with the first or last term in the time series y and could be obtained through Eq. (5):

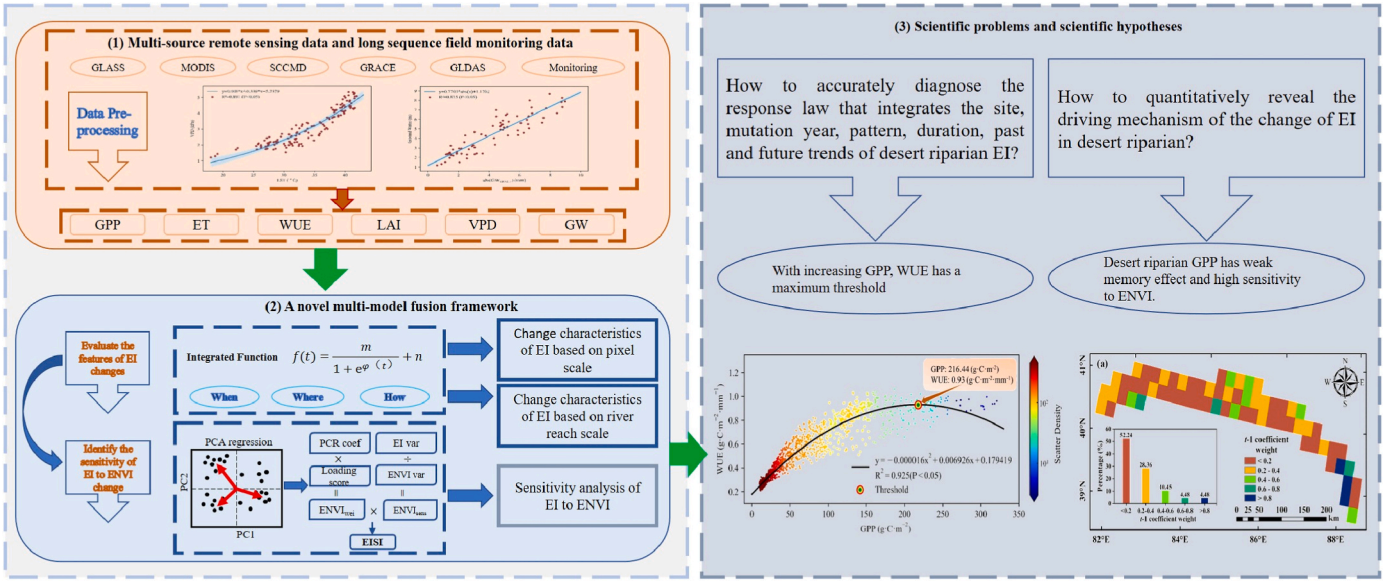

Fig. 2. The overall framework of the study. (EI is the abbreviation of ecological indicator, and ENVI is the abbreviation of ecological environmental factor).

$$L=\begin{cases} n & P=n/2 \\ 2\times(n-P) & P<n/2 \\ 2\times(P-1) & P>n/2 \end{cases} \quad (5)$$

Next, the integration function is used to fit the time series k:

$$f(t)=\frac{m}{1+e^{\varphi t}}+n \quad (6)$$

where parameter m is the difference between the maximum value of the time series and the background value, representing the change intensity of ecological indicators in a certain time duration (Cao et al., 2015). When $\varphi(t)=p(t-q)$, Eq. (6) is equivalent to the logistic function (Zhang et al., 2003). In another case, when $\varphi(t)=p(t-q)^2$, Eq. (6) is equivalent to the asymmetric Gaussian function (Jonsson and Eklundh, 2002). Note that parameter p indicates the direction of ecological indicator change, and parameter q indicates the time when the change occurs. The goodness of fit is determined by the F statistical test. "Mutation year" refers to the year when an ecological indicator abruptly starts or finishes changing. The start of a change is generally caused by a disturbance event, and the end of a change indicates that the change in an ecological indicator has reached a stable state. In this study, the change rate of curvature method was used to identify the mutation points. The change rate K of the integration function can be expressed by Eq. (7).

$$K=\frac{-m\times e^{\varphi(t)}\times\varphi'(t)}{\left[1+e^{\varphi(t)}\right]^2} \quad (7)$$

The first-order derivative of K is then calculated and the position of the mutation point is the corresponding point of the maximum and minimum values. Through the number of mutation points and the four parameters of the integration function, eight nonlinear change patterns of ecological indicators can be identified (as shown in Table S2).

As for the pixels that did not pass the F-test and those without transition years, we could use Eq. (8) to fit the series y.

$$f(i)=s+slope\times i \quad i=1,2,\cdots,n \quad (8)$$

where i is the i-th year in the series y of ecological indicators; s and $slope$ are linear regression parameters; and $slope$ represents the change trend of ecological indicators. The F-test was also used to determine the goodness of fit. The ecological indicators of the grid points that passed the F-test showed a linear change trend, whereas the other grid points that did not belong to the above patterns were defined as having no obvious change trend and were not analyzed in detail in this study. In addition, to verify whether a linear change pattern also had a mutation point, the Mann-Kendall mutation test was used. First, the Mann-Kendall test order column was constructed:

$$S_k=\sum_{i=1}^{k}\sum_{j=1}^{i}\alpha_{ij}\ (k=1,2,3,\ldots,n)\ \alpha_{ij}=\begin{cases}1 & x_i>x_j\\ 0 & x_i\le x_j\end{cases} \quad (9)$$

Under the assumption of random independence of time series, S_k was normalized to UF_k. For a given significance level α, if $|UF_k|>U_\alpha$, this suggests that the series has an obvious change trend. Take the opposite of the series of UF_k and get its inverse series UB_k. If the curves UF_k and UB_k intersect and the intersection is between the critical lines, the time corresponding to the intersection is the year when the changeover began.

This module can automatically identify the five ecological indicator change patterns of linear, exponential, logarithmic, logistic, and Gaussian. The positive and negative trends of these five patterns were classified into ten cases, as shown in Table S2. Finally, the parameters in the function were used to evaluate the characteristics of ecological indicator change, including the time (when), place (where), and pattern (how) of change. Fig. S2 details the technical flowchart of the module (1). Note that no Gaussian change patterns were detected during pixel and reach scale analysis, and therefore only eight change patterns will be discussed in the following analysis.

2.3.2. Identifying the sensitivity of ecological indicators to environmental change

A novel empirical method developed by Seddon et al. (2016) can quantify the sensitivity of different regions to climate change. This study will use this method to explore the impact of a changing environment on ecological indicators and then reveal the driving mechanism for these changes (Fig. S3). In this study, three environmental variables, LAI, VPD, and GW, were used. And the ecological indicator data with a lag of one month were used as the fourth variable in the regression to study the potential impact of the memory effect on driving ecological indicator dynamics. First, to remove the seasonal components in the annual time series, the annual data were de-trended and then standardized using the Z-score normalization formula:

$$Z_i=\frac{x_i-\overline{x_i}}{\sigma_i} \quad (10)$$

where x_i is the detrended data in the i-th year and $\overline{x_i}$ and σ_i are the mean and standard deviation of the variable x in all years, respectively. Next, the ARI multiple regression method was used to calculate the linear relationship between ecological indicators and environmental variables and the influence of the memory effect on each pixel:

$$EI_t=\alpha\times EI_{t-1}+\beta\times LAI_t+\gamma\times VPD_t+\delta\times GW_t+\varepsilon_t \quad (11)$$

where EI_t is the standardized ecological indicator value (GPP or ET or WUE) at time t and EI_{t-1} is the abnormal standardized ecological indicator (GPP or ET or WUE) at time t-1. LAI_t, VPD_t, and GW_t are standardized LAI, VPD, and GW at time t, respectively. ε_t is the residual term at time t, and α, β, γ, and δ are the LAI, VPD, GW, and EI_{t-1} coefficients of each pixel, respectively. Compared with the correlation coefficient, which can only reflect whether the ecosystem responds to environmental variability, the regression coefficient can further reflect the response amplitude. To eliminate collinearity among the four variables, principal component regression (PCR) was applied within each pixel to quantify the relative importance of each variable in driving changes in ecological indicators. Principal components that were significantly related to the environment ($p<0.1$) were selected. The load scores of each variable were then multiplied by the PCR coefficients, and the results were added up to estimate the relative importance of each variable in driving interannual changes in ecological indicators.

2.4. Structural equation model

The structural equation model (SEM) is a comprehensive statistical analysis method combining factor analysis and path analysis. It has many advantages that traditional statistical analysis methods do not have: it can not only study the internal structure relationship of variables, but also study the relationship between variables, allowing for error and measuring multiple variables. Therefore, this study used the structure function model to study the correlation between ecological indicators and environmental factors, and whether correlation between environmental factors exists. By combining this approach with the sensitivity analysis, the driving mechanism of change patterns can be better analyzed.

3. Results and analysis

3.1. Change characteristics of ecological indicators based on pixel scale

Among the GPP change patterns (Fig. 3a), linear change (67.70%) is the most common, and the linear decreasing pattern accounts for the largest percentage (35.62%) of the eight change patterns. This type of pattern is mainly distributed in the desert area of the basin. The percentage of linear growth pattern is the highest among all growth patterns, at 32.10%. Among the other change patterns, the percentages of exponential growth, exponential decrease, logarithmic growth,

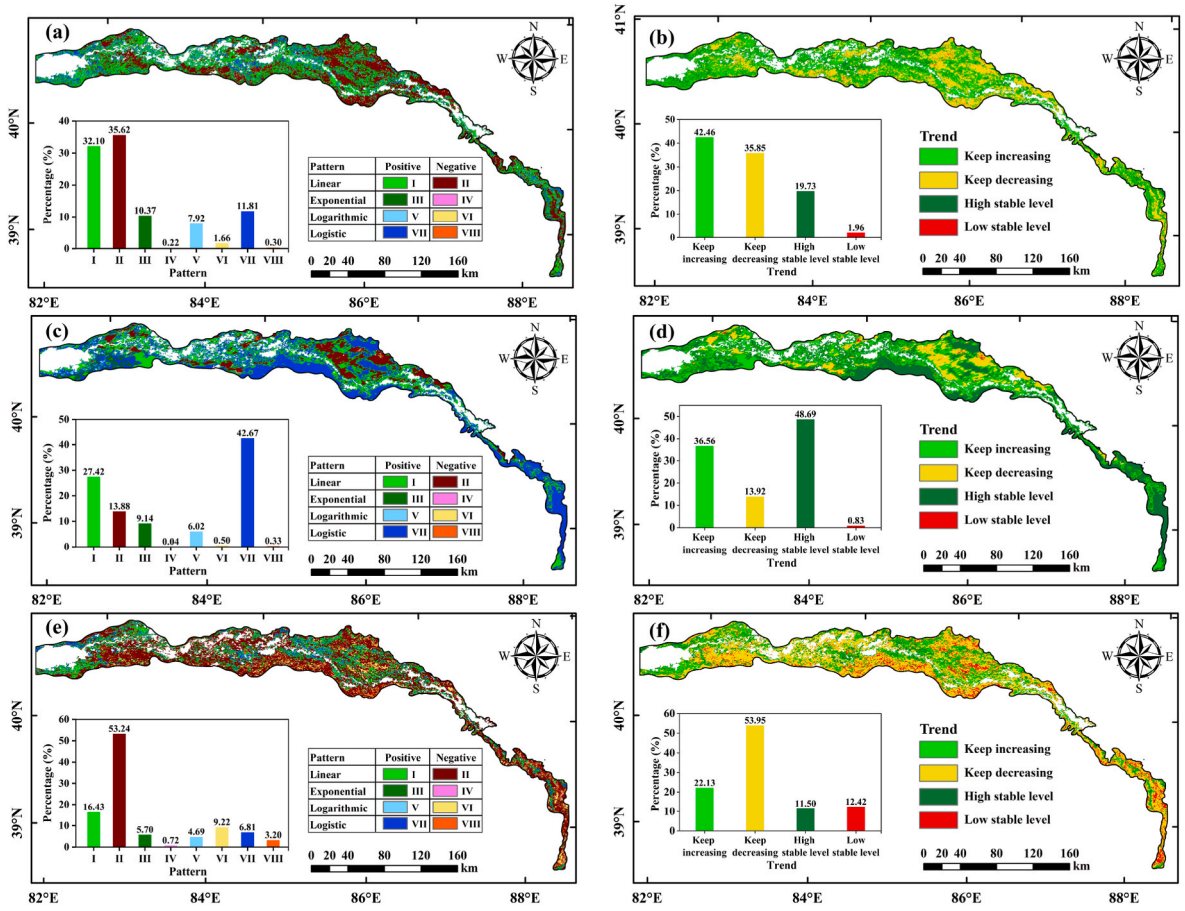

Fig. 3. The spatial distribution of gradual change pattern (a, c, e), and future change trend (b, d, f) of GPP, ET and WUE, respectively, in the Tarim River Basin during the period 2001–2018. There are four patterns: linear pattern, exponential pattern, logarithmic pattern, and logistic pattern. Each pattern is further divided into two types: positive and negative pattern. The future trend includes: keep increasing, keep decreasing, high stable level and low stable level.

logarithmic decrease, logistical growth, and logistical decrease were 10.37%, 0.22%, 7.92%, 1.66%, 11.81%, and 0.30%, respectively. In terms of overall trend, the percentage of the area with an upward trend (62.20%) was higher than the percentage with a downward trend (37.80%). As for future change trends in GPP (Fig. 3b), the area with continuous increasing GPP trend accounted for the highest percentage (42.46%); the percentage of the area with a low level of stability was the lowest (1.96%). In the future, areas with decreasing trend (35.85%) will be mainly desert, followed by grassland vegetation. Accordingly, the future change trend of GPP is that the area percentage of continuous improvement and high-level stable state (62.20%) will be higher than that of continuous deterioration and low-level stable state (37.80%). GPP is generally in or tends to be in a benign state.

Fig. 3c shows the spatial distribution of ET change patterns. Among all change patterns, the logistical growth pattern dominated (42.67%), and the bare desert land in the Tarim River Basin mainly presented this change pattern. Among all the negative change patterns, the linear decreasing pattern accounted for the highest percentage (13.88%). Overall, the percentage of the growth pattern (85.25%) was much larger than that of the decreasing pattern (14.75%). The decreasing patterns were most intensively distributed in the midstream reach, with only a few in the upstream reach. As for the future development trend of ET (Fig. 3d), areas in a high-level stable state accounted for the highest percentage (48.69%), and the areas in a low-level stable state accounted for the lowest (0.83%). In the future, ET in a few areas of the midstream and upstream reaches will continue to decrease (13.92%). In general, the percentage of pixel area where ET continues to rise or is in a high-level stable state (85.25%) is much larger than the percentage where ET continues to decrease or is in a low-level stable state (14.75%), indicating that ET will continue to rise or maintain a high value.

Fig. 3e shows the spatial distribution of WUE change patterns. The linear decreasing pattern accounted for 53.24%, which is far more than other change patterns, and was concentrated in the bare desert land in the Tarim River Basin. In general, the percentage of pixel area with a negative WUE trend (66.37%) was higher than the percentage with a positive trend (33.63%), and the distribution area of positive WUE pattern in the upstream and midstream reaches was larger than in the downstream reach. From the perspective of future WUE trends (Fig. 3f), WUE in more than half the area will continue to decrease (53.95%), with the areas in a high-level stable state accounting for the lowest percentage (11.50%). WUE in most areas of the Tarim River Basin can be expected to continue to decrease or to maintain a low-level stable state (66.37%), whereas the areas where WUE will continue to improve or to maintain a high-level stable state are mainly distributed in the upstream and midstream reaches (33.63%).

The research method in this study can also detect the mutation point of linear patterns. Among all the pixels of GPP, ET, and WUE, the percentages of pixels with a mutation point were 58.25%, 70.81%, and 49.04% respectively (Fig. S4). In terms of the occurrence year of the first GPP mutation point (Fig. S5a), since 2000, the percentage of pixels undergoing transformation has generally shown an increasing trend with time, and the transformation year of the upstream and downstream reaches was generally earlier than that of the midstream reach. 2014–2016 was the main period of GPP transformation, during which the percentage of pixels that changed was 50.52%, mainly distributed in the midstream reach. The first mutation point of ET, appearing in 2012,

accounted for 38.23% of pixels and was concentrated in the midstream and downstream reaches (Fig. S5b). The first mutation point of WUE generally appeared from 2014 to 2016. During this period, transition pixels were widely distributed in the upstream and midstream reaches, accounting for 42.30% of all pixels (Fig. S5c).

The logistic change pattern reached a relatively stable state after the second mutation point, and the spatial distribution of the year at the second mutation point is shown in Figs. S5d–S5f. For GPP change (Fig. S5d), the percentage of stable regional area showed a significantly increasing trend from 2010 to 2018, and the percentage of total pixel area reached 81.73% during this period. The second ET mutation point was mostly in 2013, with a continuous lamellar distribution in the midstream and downstream reaches (Fig. S5e). WUE stopped changing mainly from 2011 to 2016, and the area of the pixels where WUE stopped changing during this period accounted for 83.46% of total pixel area (Fig. S5f).

According to the results, the longest duration of the logical change pattern in the Tarim River Basin was 15 years. The study divided 15 years of continuous change into four types: less than two years, three to four years, five to seven years, and eight years or more. The spatial distributions of the duration of change of GPP, ET, and WUE are shown in Figs. S5g–S5i. In Fig. S5g, the percentage of duration of change of GPP within 2 years is the highest, reaching 33.95%, followed by change taking more than 8 years, which accounted for 26.19%, and change taking 3–4 years with the lowest percentage, 14.45%. The highest percentage of ET change duration in Fig. S5h is also 1–2 years, accounting for 63.51% of pixels, and the lowest percentage is more than 8 years, accounting for 9.64%. In Fig. S5i, the highest percentage of WUE change duration is more than 8 years, accounting for 38.41%, followed by 1–2 years (28.11%), and 3–4 years (11.31%). The spatial distributions of the change durations of GPP and WUE showed obvious spatial heterogeneity, but the pixel distribution of ET change lasting less than 2 years had spatial continuity, these changes were mainly distributed in the midstream and downstream reaches.

3.2. Change characteristics of ecological indicators based on reach scale

After all the pixel values in each year had been averaged, the change pattern of the whole region was obtained using the proposed framework (Figs. 4–6). As can be seen in Fig. 4, GPP in the mainstream, upstream, midstream, and downstream reaches of the Tarim River all showed an upward trend from 1982 to 2018. Among them, only the upstream change pattern was a logistic growth type, which began to change significantly in 1990 and became stable in 2011. The change patterns of the other reaches were all exponential growth, and the years of abrupt change points in the upstream, midstream, and downstream reaches were 1996, 2002, and 2001, respectively. The overall average GPP decreased gradually from upstream to downstream.

Fig. 5 shows that ET in the mainstream, upstream, midstream, and downstream reaches all showed a positive trend from 1982 to 2018. Among these, the changes in ET in the mainstream and midstream reaches both showed exponential growth, and their transformation years were 1999 and 2001 respectively. Both upstream and downstream ET showed a logistic increase pattern. Their first transition points were in 1986 and 1998, respectively, and the changes started to stabilize in 2000 and 2013, respectively.

As for the regional change patterns of WUE (Fig. 6), the WUE of the mainstream, upstream, midstream, and downstream reaches all showed an exponential growth trend from 1982 to 2018, whereas the WUE of pixels with more than 50% area in Fig. 3g showed a downward trend. The significance test of WUE change mode of each pixel showed that 41.22% of the pixels in the decreasing mode had no significant change

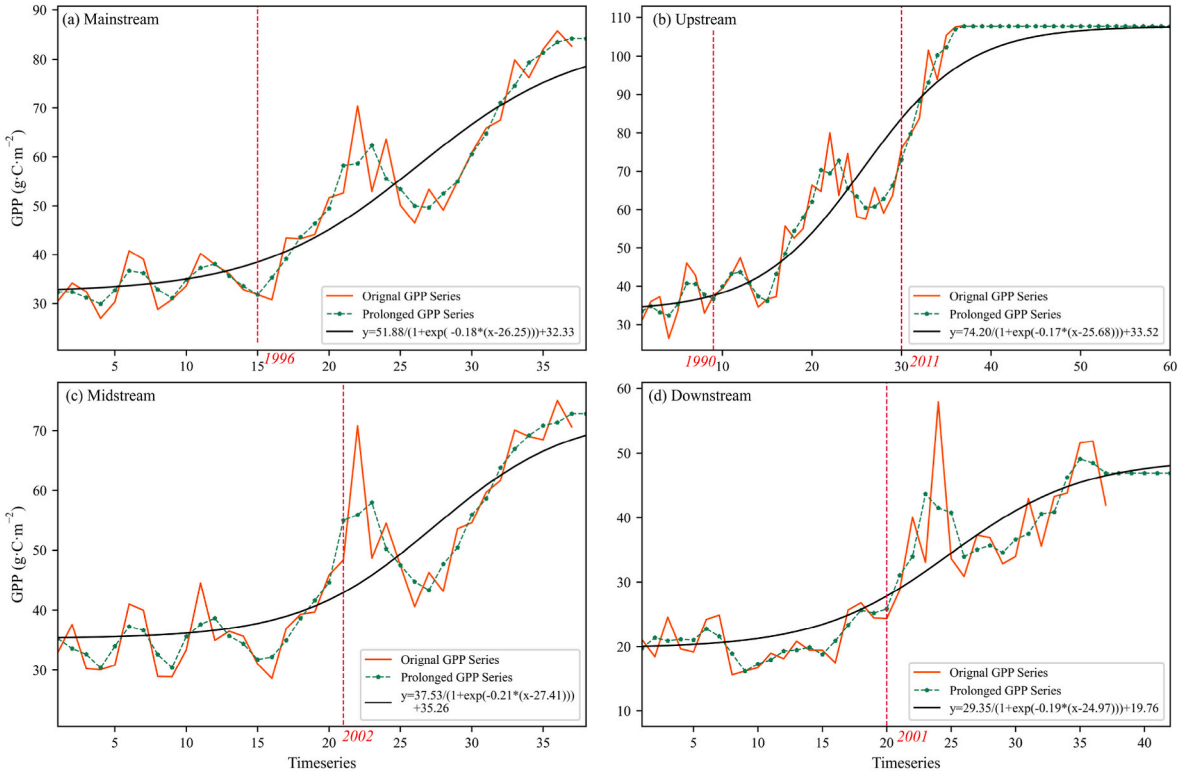

Fig. 4. Processes of GPP gradual change pattern in four regions from 1982 to 2018. (a: Mainstream; b: Upstream; c: Midstream; d: Downstream).The contents of each subfigure include profiles of the original GPP timeseries (orange solid line), the prolonged timeseries (green dotted line), the fitting temporal profile (black line), and the time of the transition point (red word). Values in the horizontal axis in each subgraph represent the serial numbers in the prolonged timeseries (k) which ranges from 1 to L while that in the vertical axis are mean April to October GPP. (For interpretation of the references to colour in this figure legend, the reader is referred to the Web version of this article.)

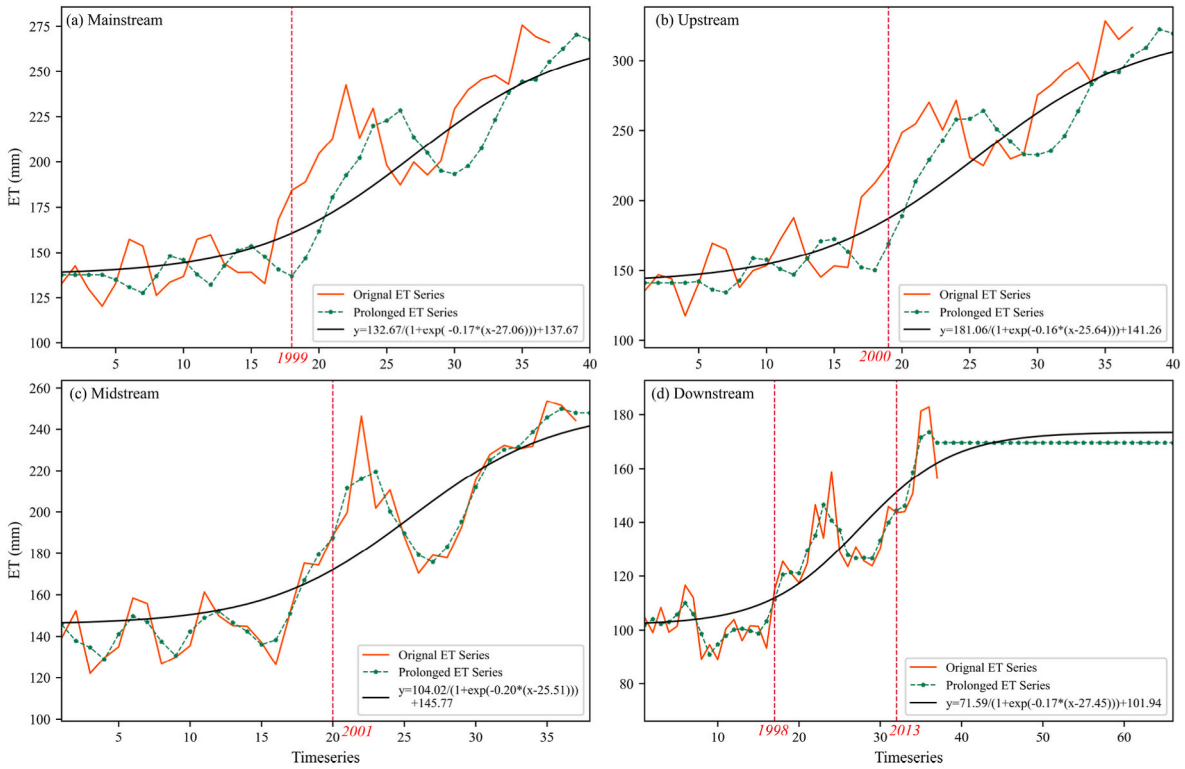

Fig. 5. Processes of ET gradual changing pattern in four regions from 1982 to 2018. (a: Mainstream; b: Upstream; c: Midstream; d: Downstream). The contents of each subfigure include profiles of the original ET timeseries (orange solid line), the prolonged timeseries (green dotted line), the fitting temporal profile (black line), and the time of the transition point (red word). Values in the horizontal axis in each subgraph represent the serial numbers in the prolonged timeseries (k) which ranges from 1 to L while that in the vertical axis are mean April to October ETs. (For interpretation of the references to colour in this figure legend, the reader is referred to the Web version of this article.)

and that 53.86% of the pixels in the linear decreasing mode had no significant downward trend (Table S3). The variation range of WUE in the Tarim River Basin from 1982 to 2018 was approximately 0.2–0.3. WUE in the four regions remained relatively stable before 2000, but increased significantly after 2000. The years of the transition points were 2003, 2007, 2008 and 2005, respectively.

3.3. Sensitivity analysis of ecological indicators to environmental change

The regions where GPP, ET, and WUE responded to changes in the three variables (LAI, GW, VPD) with amplification were first identified by calculating the sensitivity index (Fig. S6). GPP had the strongest sensitivity overall, followed by ET, and WUE was the weakest. Specifically, the area of pixels with a GPP sensitivity index greater than 50 accounted for 83.58% of the total; weak sensitivity (sensitivity index less than 50) generally appeared in desert areas; the overall sensitivity of GPP in the upstream southwestern regions was strong, and its sensitivity index remained above 60 (Fig. S6a). The area of pixels with ET sensitivity index less than 50 accounted for 64.14% of the total, and the ET in the upstream southwestern region also showed strong sensitivity (Fig. S6b). The percentage of pixel area with WUE sensitivity index less than 40 was 74.63% (Fig. S6c). In particular, overall WUE sensitivity in the midstream reach was relatively low.

The relative contribution of each variable to sensitivity was also evaluated (Fig. S7). GPP was the most sensitive to LAI changes. The regions driven by GW were mainly in the upstream and midstream reaches (Fig. S7a). The downstream area was mainly affected by the combination of LAI and VPD. ET also showed a high sensitivity to LAI. The upstream reach and the first half of the midstream reach were mainly affected by the combination of LAI and VPD, whereas the transition zone between the midstream and downstream reaches reacted strongly to GW changes (Fig. S7b). WUE was the most sensitive to changes in GW, especially in the upstream region. WUE in the midstream and downstream reaches was mainly driven by the combination of the three factors (Fig. S7c).

The greater the weight of the *t*-1 coefficient, the stronger will be the memory effect. As shown in Fig. S8a, GPP in almost the entire study area showed a relatively weak memory effect ($\alpha < 0.4$), with an area percentage of 80.60%. From the upstream to the downstream reaches, the memory effect of GPP gradually increased. ET also showed a relatively weak memory effect in general, with the area with $\alpha < 0.4$ accounting for 63.63% of the pixels in the study area. The memory effect of ET in the midstream and downstream reaches was generally stronger than in the upstream reaches (Fig. S8b). Compared with GPP and ET, WUE showed a stronger memory effect. The area percentage with $\alpha > 0.4$ of WUE was 53.73%, and the overall memory effect downstream was stronger than that midstream and upstream (Fig. S8c).

4. Discussion

4.1. Driving process of the change pattern of ecological indicators

In the mainstream, upstream, midstream, and downstream of the Tarim River Basin, GPP, ET, and WUE have shown an overall increasing trend since 1982 (Figs. 4–6). Many other researchers have found similar patterns when studying arid and semi-arid systems globally (Ichii et al., 2013; Zhang et al., 2020). To analyze the reasons for this change in depth, a structural function model was constructed to study it.

According to the results of the structure equation model (Fig. 7), LAI has a significant positive impact on changes in GPP, ET, and WUE. As a characteristic parameter of vegetation growth conditions, LAI can reflect the level of vegetation coverage. LAI increases the amount of

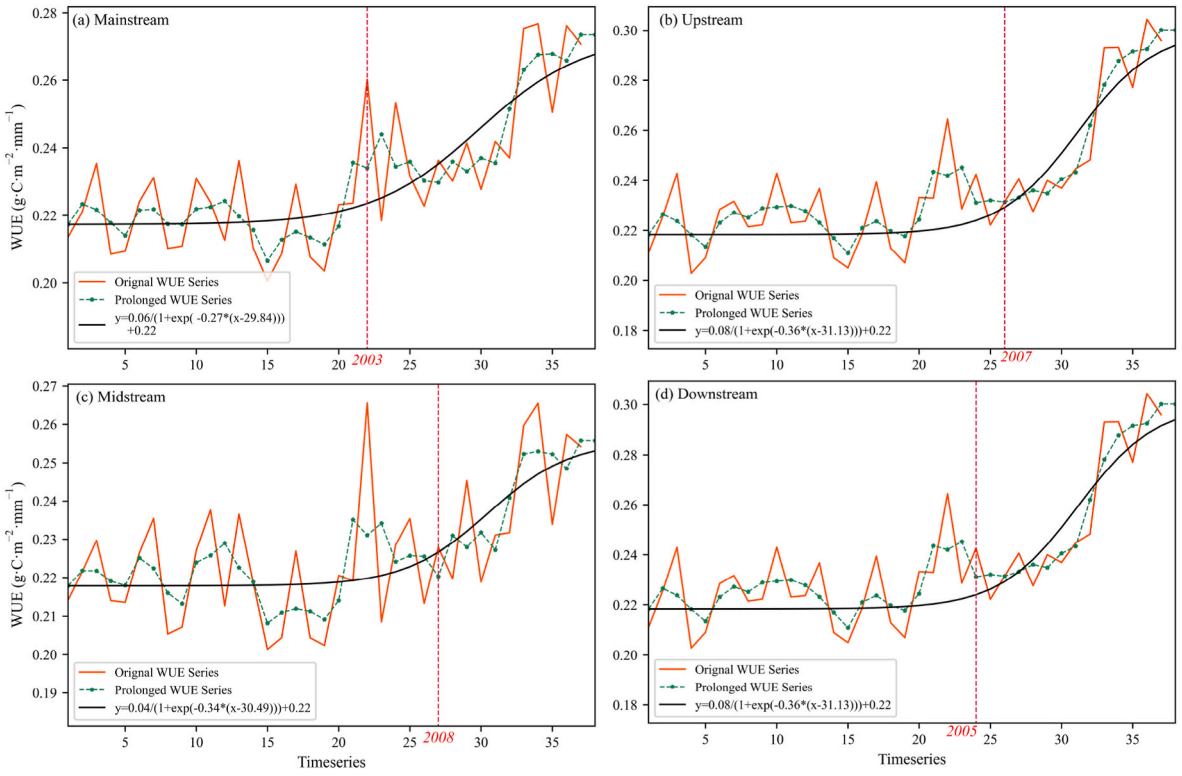

Fig. 6. Processes of WUE gradual changing pattern in four regions from 1982 to 2018. (a: Mainstream; b: Upstream; c: Midstream; d: Downstream). The contents of each subfigure include profiles of the original WUE timeseries (orange solid line), the prolonged timeseries (green dotted line), the fitting temporal profile (black line), and the time of the transition point (red word). Values in the horizontal axis in each subgraph represent the serial numbers in the prolonged timeseries (k) which ranges from 1 to L while that in the vertical axis are mean April to October WUEs. (For interpretation of the references to colour in this figure legend, the reader is referred to the Web version of this article.)

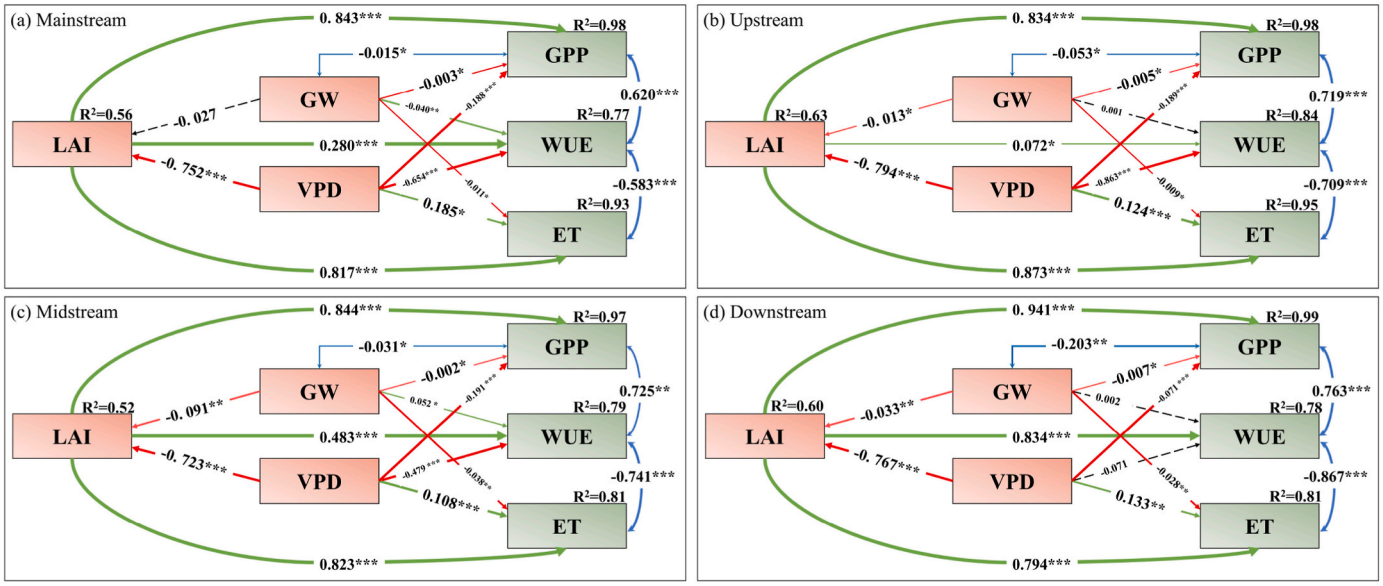

Fig. 7. The results of structure equation model. (a: Mainstream; b: Upstream; c: Midstream; d: Downstream).

photosynthetically active sunlight that is absorbed by vegetation, thus enhancing productivity (Chen et al., 2019). LAI can also control the transpiration of vegetation and is therefore closely related to changes in ET. In this study, VPD has a negative effect on GPP, but a positive effect on ET. According to Yuan et al. (2019), an increase in VPD would lead to partial stomatal closure and inhibit photosynthesis and transpiration rate, thus decreasing GPP and ET. However, our study showed the opposite for ET. ET includes two main kinds of water loss: productive water consumed by plant transpiration, and unproductive water lost by soil evaporation and canopy interception (Sun et al., 2016). The conclusion of this study is mainly due to the increase of soil evaporation when the temperature-driven vapor pressure loss increases. In addition, VPD can also indirectly inhibit the increase in GPP through a direct negative effect on LAI. Chen et al. (2020) found that VPD controls the

fall of old leaves, thus driving a dynamic change in the leaf area index. Groundwater (GW) depth has a direct negative effect on changes in GPP and ET. Groundwater is the main source of maintaining the existing structure and function of the landscape in hyper-arid areas (Madani et al., 2020). Under limited water supply condition, groundwater supports primary productivity by improving soil water availability (Madani et al., 2020). Many studies have also shown a positive correlation between groundwater depth and productivity in arid ecosystems (Kochendorfer et al., 2011; Scott et al., 2006). The shallower the groundwater depth, the more effectively water can be provided for plant transpiration and soil evaporation, and therefore ET will be greater. As for WUE, the positive or negative impacts of various environmental variables on it depend on the magnitude and direction of their relative impacts on GPP and ET. In comparison, GPP in the Tarim River Basin has the strongest correlation with LAI and is the most sensitive to LAI change (Fig. S7a). Therefore, LAI is the main controlling factor for GPP change in the Tarim River Basin.

The model can explain more than 97% of GPP changes in the mainstream, upstream, midstream, and downstream regions (Fig. 7). Although the increase in VPD (Fig. S9d) in the downstream reach had a negative effect on GPP, the correlation coefficient between VPD and GPP was very small. The increase in GW (Fig. S10b) in the upstream reach had a negative effect on GPP, but the correlation coefficient between the two was only 0.005, meaning that the negative effect on GPP change was small. Therefore, the GPP in the four regions eventually rose gradually (Fig. 4) because LAI in these four regions showed an upward trend (Fig. S11), Among the three factors, LAI has the highest correlation with ET and dominated the changes in ET. Increasing LAI will promote plant transpiration, and decreasing VPD will reduce soil evaporation. However, with decreasing groundwater depth, the corresponding water supply will increase, accentuating vegetation transpiration and soil evaporation. Therefore, ET eventually showed an upward trend (Fig. 5). The increasing trend of WUE in the four regions (Fig. 6) can be explained as follows: the increasing trend of WUE in the mainstream and upstream reaches was mainly controlled by the decreasing trend in VPD; the increasing trend of WUE in the midstream reach was mainly affected by the combined impact of the gradual increase in LAI and the continuous decrease in VPD; the change of WUE in the downstream reach was dominated by the rising trend in LAI. From the spatial distribution perspective, the percentage of pixel area with increasing trends of GPP and ET is greater than the percentage with a decreasing trend (Fig. 3a and c), which is consistent with the positive trend of regional change patterns (Figs. 4 and 5). The percentage of pixel area with a decreasing WUE trend (66.37%) was higher than the percentage with an increasing trend (33.63%) (Fig. 3e). However, the downward trend of 62.11% of the pixels was not significant (Table S3), and therefore, the increasing trend in regional WUE (Fig. 6) does not contradict it. Comparing the regional change trends of GPP and WUE (Figs. 4 and 6), WUE changed very gently before the mutation, and its transition point generally appeared later than that for GPP. This may have occurred because the comprehensive sensitivity of WUE to the three variables was very weak (Fig. S6c). Meanwhile, the memory effect for WUE was also stronger than that for GPP (the percentage of pixels with WUE's t-1 coefficient weight less than 0.4 was much lower than for GPP, as shown in Fig. S8). As a result, when the ecosystem is faced with external disturbances, vegetation has a lagging response to water utilization and makes timely adjustments to the changing environment. This is manifested as the phenomenon that WUE remains stable for some time after human interference and the mutation year is overall later than for GPP.

As for the regional GPP change pattern, the whole mainstream reach is still in the continuous rising stage (Fig. 4a). Therefore, it is necessary to strengthen the reconstruction of the Tarim River Basin to promote further development and restoration of the ecosystem. The upstream area has the largest inflow and a good water regime, and the vegetation has the fastest response to the ecological water supply and the best growth, so that the upstream GPP has reached a stable state (Fig. 4b). In the future, minimal attention will be needed in this area, but efforts should focus on protection. GPP in the midstream region has moved from a stable period to a continuous acceleration period since 2002 and is expected to show a benign development trend (Fig. 4c). Therefore, the midstream reaches of the basin should be a focus of attention, and restoration efforts should be intensified. Theoretically, the effect of ecological water supply shows a lagging process from upstream to downstream. However, the rise of downstream GPP is likely to stabilize gradually (Fig. 4c), which is related to the focus on downstream regions in recent years. The change patterns of GPP in different zones are consistent with hydrological conditions and prove the correctness of the proposed method.

4.2. Performance and advantages of the novel multi-model fusion framework

The emergence of high-resolution satellite remote-sensing time-series products provides an opportunity to study dynamic changes in ecological indicator time profiles. In this study, multi-source remote-sensing data and actual monitoring data were used for research, including GLASS finished product data, MODIS data, GRACE satellite data, GLDAS data, and measured groundwater depth data. The data set was large and comprehensive, and data accuracy was further improved by inversion correction. To calculate VPD, LST data were used to reconstruct the missing pixels of RH data and to correct the VPD calculation results. In addition, the groundwater depth data obtained by remote-sensing inversion were corrected by measured groundwater depth data, improving their accuracy.

At present, the trend analysis method is widely used to study the change law of ecological indicators. The trend analysis method is simple, effective, and clear. Univariate linear regression analysis is the most popular method. However, this method is a parametric method. Only when the four preconditions are strictly met can the slope value estimated by this method accurately represent the annual average change rate of ecological indicators in the study period (Wessels et al., 2012). Although the Theil-Sen method and the Mann-Kendall trend analysis method require no assumptions, the Theil-Sen method can only estimate the median slope of a time series and cannot test the significance of the results, whereas Mann-Kendall trend analysis can determine the overall change direction of a time series, but cannot determine any information about the change magnitude for ecological indicators. The simple trend analysis method can generally be used to clarify change location, direction, and amount, but it cannot fully extract detailed change information about ecological indicators that is hidden in the time-series trajectory. In view of the shortcomings of trend analysis methods, new detection methods have been developed, including the breakpoint detection algorithm and the trend decomposition method. The DBEST method is currently widely used in the breakpoint detection algorithm. This method often requires manual setting of important parameters to determine the major feature points in a time series, such as change threshold, change duration, and number of breakpoints (Jamali et al., 2015). Therefore, it is difficult to achieve automatic extraction of long-term change information for ecological indicators. The BFAST method is a representative trend decomposition method and has been widely used to analyze the long-term change process of ecological indicators (Fang et al., 2018). However, due to the different numbers of breakpoints detected in the remote-sensing time series for different pixels, it is difficult to generalize the decomposed trend components into an easily understood pattern, which makes it difficult to carry out comparative analysis of the change process of ecological indicators between pixels or regions.

Therefore, some researchers have tried to find a more universal method to study the change process of ecological indicators under a changing environment. In recent years, the application of time-series trajectory detection methods to detect changes in ecological indicators has aroused more and more research interest. Among these, the logistic

function is widely used to fit vegetation index time series to estimate the phenological date of vegetation. Verification shows that the model has high accuracy (Cao et al., 2015). Specifically, a new function integrating the logistic function and an asymmetric Gaussian function has been used to fit LAI data to determine the end date of the growing season (EGS) (Che et al., 2014). Validation results show that the inversion results of EGS are highly consistent with the minimum observed values of the autumn GPP (Che et al., 2014). This study is encouraging: to simplify the steps, existing relevant research usually considers only monotonic change processes of ecological indicators, ignoring more complex changes. However, the integration function used in this study can not only fit the monotonic logistic change process conforming to ecological significance, but can also consider a non-monotonic Gaussian function change process in which ecological indicators undergo degradation after restoration or the reverse. To improve the testing ability of our model, the new integration function was adopted to detect change processes in ecological indicators. Compared with the single logistic function and the asymmetric Gaussian function, the ensemble function showed better fitting performance and recognition ability (Che et al., 2014), providing a more comprehensive analysis method for exploring the dynamic process of ecological indicators after an ecosystem has been disturbed.

This study is the first to apply the new function integrating the four-parameter logistic function and the asymmetric Gaussian function to the nonlinear fitting of vegetation GPP, ET, and WUE changes and to use linear regression to fit the linear change trend. The proposed method is improved in the following two main aspects: the Gaussian function is combined with the logistic function to fit the nonlinear change trend, so that the introduced Gaussian function can add a new change pattern (Gaussian) beyond the three change patterns (exponential, logarithmic, and logistic) fitted by the logistic function. This enables the method to detect non-monotonic changes, such as the decline of ecological indicators after restoration, or the reverse. Because mutation points occurred in some linear patterns, the Mann-Kendall mutation test was used to test these points. By extending the data time series according to its recent change trend, the proposed model can predict future change trends, which effectively solves the problem encountered in previous studies, that future development trends could not be predicted.

Compared with the trend analysis method, the method proposed here can automatically track the trajectory curves of changes in ecological indicators and obtain detailed information such as the time and duration of disturbance events according to the model parameters. Thus, it can comprehensively detect the long-term change process of ecological indicators. In addition, because the time series has been smoothed, it is easier for the simulated curve to pass the significance test, thus detecting a wider range of areas of significant variation. In general, the method proposed in this paper has the following advantages. First, no threshold or empirical constant needs to be set separately when processing each pixel, which renders pixel analysis easy to implement, making this method globally applicable. The method can also reduce the uncertainty caused by human subjective factors. In addition, this model can not only detect linear change trends, but also identify monotonic and non-monotonic nonlinear change trends, and all change patterns can be explained from a clear biophysical perspective. Finally, although the proposed method uses only one function form, it integrates four functions (exponential, logarithmic, logistic, and Gaussian) without setting other complex functions, which simplifies the calculation steps and makes detection by the model simple and convenient.

The basic problem in time series-based change detection is evaluating the method. The proposed framework is designed on the basis that the temporal trajectories of ecological indicators will alter after a major disturbance event. Temporal evidence of abrupt changes in ecological indicators at pixel and reach scales was used to assess the effectiveness of this method. For example, in the Tarim River Basin, there is good consistency between the mutation year detected in the GPP change pattern and the implementation time of major initiatives. On the pixel analysis scale, the mutation years of GPP, ET, and WUE are mostly concentrated after 2011 (Figs. S5a–S5f), which is consistent with the time that unified management of four-source flow was instituted. On the reach scale, the first sudden change of GPP in the upstream reach occurred in 1990 (Fig. 4b), which is the year when the Tarim River Basin Authority was established to begin overall management of the mainstream reach and strengthen water management practices. The GPP in the upstream reach attained a stable level in 2011 (Fig. 4b), which is in line with the time when the four sources and one trunk of the Tarim River Basin were placed under the oversight of the Tarim River Basin Authority for unified management to ensure ecological use of mainstream water resources. The years of GPP mutation in the midstream and downstream reaches were 2002 and 2001 respectively (Fig. 4c and d), which is close to the time when the Tarim River Basin began to implement ecological water transportation in 2001. These examples demonstrate the accuracy of this method, which can accurately detect abrupt disturbances in the long-term change process of ecological indicators.

However, an optimal detection method should be able to completely depict all the characteristics of the long-term changes of ecological indicators. It should not only identify where, how, when, and what ecological indicators have changed, but also explain the reasons for such changes. Therefore, how to build a framework that can comprehensively detect the long-term change process of ecological indicators and identify its driving mechanism has become an urgent problem to be solved in this research field. Changes in ecological indicators are the result of the combined effects of various factors, and the mechanisms of action are very complicated. This study has attempted to fully analyze the reasons for the changes by seeking fewer variables. Therefore, ecological changes were considered from the three aspects of physiology, environment, and hydrology, and a representative index was selected for each aspect to comprehensively characterize environmental changes and to study how these changes drive the changes in ecological indicators.

In the early stage, quantitative research on the relationship between ecological indicators and environmental changes aimed mainly to study the consistency between ecological and climatic indicators by comparing the annual variation trajectory curves of ecological and climatic indicators, with the objective of determining the dominant factors affecting changes in ecological indicators. Based on remote-sensing parameter time-series data, many researchers have quantified the relationships between global or regional changes in ecological indicators and climate factors by the coefficients or parameters in the linear regression model (Zhao et al., 2021). Among the applicable methods, correlation analysis should be the most widely used. For example, the Pearson, Spearman, and Kendall methods can reveal the degree of correlation between two variables (Keenan et al., 2013); the partial correlation coefficient of each environmental factor can be calculated by controlling other factors to reveal the relationships between changes in ecological indicators and specific environmental factors (Liu et al., 2020; Beer et al., 2010); multivariate correlation analysis can be used to explain the response of ecological indicators to changes in various environmental factors (Sun et al., 2016; Zhang et al., 2020). However, these methods only seek the average response relationship between ecological indicators and various driving factors, and there are often differences in the degree of response of ecological indicators in different regions. Therefore, the spatial pattern of the response of ecological indicators to different factors should be clearly expressed. The variation in the spatial distribution of the contribution rate of each factor to changes in ecological indicators also needs to be given.

A sensitivity analysis method was therefore chosen to solve these problems. Through the correlation coefficient in the ARI model, the relative importance of the three environmental factors to changes in ecological indicators was determined (Seddon et al., 2016). The weight of the t-1 coefficient can be used to identify the influence of the memory effect (Seddon et al., 2016). Based on the sensitivity index, the response amplification area of ecological indicators to environmental change can

be determined, and the factors leading to changes in ecological indicators can be identified (Seddon et al., 2016).

The proposed framework detects the evolution law of ecological indicators in accordance with ecological logic under a changing environment using the integrated function, identifies the degree of response to the changing environment of ecological indicators by sensitivity analysis, and clarifies the direction of response to the changing environment of ecological indicators by introducing the structural function model. This is a comprehensive analysis framework that considers both the change law and the driving mechanism of ecological indicators. The whole process of the framework involves no specific assumptions or special requirements, making the framework universal, without clear regional restrictions. It is not only suitable for research in arid areas, but also in any other region of the world.

4.3. Important indications of GPP and WUE in water resource management

On a large spatio-temporal scale, a certain amount of water can only maintain a corresponding vegetation area, but a reasonable water transfer scheme can maximize the vegetation area corresponding to the scale of the water volume. For example, in the Tarim River Basin, GPP generally shows an upward trend (Fig. 3a), whereas WUE mainly shows a downward trend (Fig. 3e). WUE has not continued to rise due to the increase in water transmission in recent years. Relevant studies have also confirmed that ecological water conveyance in some areas near the downstream reaches of the Tarim River has reached an oversaturated state and the groundwater level has reached its highest level (Deng et al., 2017). The water consumption of soil evaporation after the groundwater rise and of lake surface evaporation after the increase in the surface elevation of Taitema Lake have both increased significantly, resulting in a gradual increase in water consumption by ineffective evaporation. However, vegetation growth in arid areas is mainly controlled by water availability (Beer et al., 2010; Jiao et al., 2021). Expanding the receiving area for water delivery will help promote vegetation growth and achieve larger areas of vegetation restoration and protection (Hu et al., 2021). Besides, due to the uneven distribution of water between reaches, there are significant differences in their ecological environmental conditions. For example, GPP in the downstream reaches of the Tarim River Basin has tended to be stable (Fig. 4d), but GPP in the midstream reaches is still in the stage of continuous growth (Fig. 4c). Similarly, China's Heihe River Basin has been practicing ecological water conveyance since 2000 (Liu et al., 2013). At present, the ecology in the downstream reaches of the Heihe River is in the stage of balanced maintenance and development, and the ecological situation has improved significantly (Liu et al., 2013). However, when the amount of water delivered is large, even the downstream reaches have overflowed many times, while the ecology of the midstream reach is seriously degraded. Therefore, any basin should be viewed as a whole, to coordinate water resource distribution and realize sustainable development of the whole basin.

In order to consolidate and improve the effect of ecological water conveyance, it is necessary to change the previous single channel water conveyance mode and introduce the ditch-branch infiltration irrigation mode in appropriate areas, controlling the amount of water entering the lake and reducing ineffective evaporation from the water surface. A ditch-branch infiltration irrigation study took China's largest inland river, the Tarim River, as its research object to construct a "double channel and gully branch" surface water conveyance mode, creating a timely, appropriate and moderate ecological irrigation mode that uses first diffuse irrigation, then infiltration irrigation, and finally rotation irrigation (Deng et al., 2020). This irrigation method is intended to maximize the limited ecological water for vegetation protection and riparian ecosystem restoration, to promote the formation and development of accurate and efficient regulation patterns of ecological water in arid areas (Deng et al., 2020). According to the ecological restoration needs and the eight change patterns presented by GPP, the areas with logarithmic and logical change patterns were regarded as an ecological protection region, where the vegetation growth was nearly stable, and the ditch-branch infiltration irrigation was mainly used to control the groundwater level (<stressed water level) to meet the ecological water demand of vegetation. The area with linear change pattern was taken as an ecologically fragile region, where the vegetation was dominated by grasses and young forests, with a focus on regulating the flood overflow process to maintain species diversity and enable young trees to become forests. The area with exponential change pattern was considered as an ecological restoration region, where adult *Populus euphratica* was the main vegetation component and the hydrological conditions were poor. The ditch-branch infiltration irrigation was adopted to raise the groundwater level and encourage the budding of *Populus euphratica* roots, combined with flood disturbance to promote seed germination (Fig. 8). In the Tarim River Basin, the areas of ecological protection, ecologically fragile, and ecological restoration regions accounted for 21.1%, 68.2%, and 10.7% respectively (Fig. 8). This refined zoning regulation approach can manage different areas more precisely, thus making regulation more purposeful and pertinent. Other basins can also carry out accurate zoning management by referring to this zoning regulation method and combining it with the actual situation of the basin itself.

Time is another key factor for successful restoration of an ecosystem (Crouzeilles et al., 2016). In the Tarim River Basin, the longest continuous change time for GPP was 15 years, which was the maximum time interval required for its ecological regulation. The durations of GPP change are mainly one to two years and more than eight years (Fig. S5g). Changes lasting for one or two years generally involve herbaceous plants, which require a shorter time for recovery or degradation. Changes with a duration greater than eight years generally involve trees and shrubs, for which the recovery process is relatively slow. From the ecological point of view, the importance of tree and shrub vegetation to the community in an arid inland river basin is greater than that of herbaceous plants. Restoration of trees and shrubs is a long-term and slow process. This means that an ecological management project cannot be completed in a short period of time. However, in the Aral Sea basin, where the problem of ecological degradation is equally serious, the five Central Asian countries cannot reach a consensus to cooperate on transboundary water. In the past 20 years, only intermittent governance has been carried out, and the Aral Sea crisis has not been fundamentally reversed (Su et al., 2021). In addition, related studies in the Heihe and

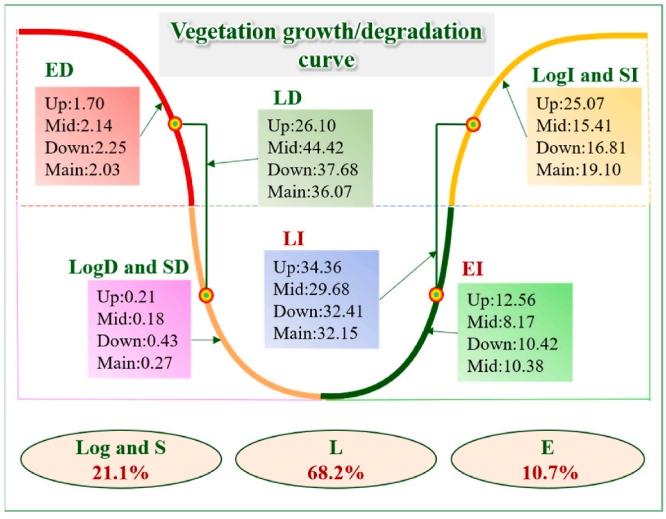

Fig. 8. Regulation zoning division of Tarim River Basin according to the change pattern of GPP. (L: Linear; E: Exponential; Log: Logarithmic; S: Logistic. D: Decreasing; I: Increasing. Main: Mainstream; Up: Upstream; Mid: Midstream; Down: Downstream).

Shiyang River Basins of China also pointed out that it will take a long time to restore the ecological environment of the basin and improve soil and water conservation (van der Meijden et al., 2010; Wang et al., 2019). Ecological restoration will not completely restore biodiversity and vegetation structure, but if there is enough time for ecological succession, old forests can be replenished, and the supplementary value of restoration helps to reduce the loss rate of biodiversity and improve vegetation structure (Crouzeilles et al., 2016).

Under multiple pressures of climate and environment such as drought, heat waves, and carbon dioxide fertilization, the structure and function of the global dryland ecosystem may undergo more drastic changes (Yao et al., 2020). All these processes interact with each other to produce nonlinear and lagging effects on the dryland ecosystem-climate cycle (Yao et al., 2020). In addition, projected increases in future drought events and environmental variability will bring further threats to ecosystems, especially in arid ecosystems with low productivity and high sensitivity (Yang et al., 2016). According to this study, GPP has the strongest comprehensive sensitivity to environmental changes among the three ecological indicators (Fig. S6). This may be related to the fact that the main type of vegetation restored in the basin is herbaceous and the overall biomass level is relatively low. Grassland is the ecosystem that responds most rapidly to environmental changes, and therefore, the loss of resilience associated with dieback will occur first (Knapp and Smith, 2001). Previous theories and studies have also shown that an intact ecosystem can compensate for its vulnerability to environmental changes (Martin and Watson, 2016), but that ecosystems close to the tipping point are more prone to collapse (Dai et al., 2012). Large-scale conservation projects contribute to greening the planet and have a positive impact on carbon sequestration (Tong et al., 2018). On a regional scale, ecological engineering projects can reduce the sensitivity of an ecosystem to environmental disturbances and reduce the risk of desertification, but only when the biomass has been restored to a certain extent by increasing vegetation cover (Tong et al., 2018). The ecological response of vegetation using groundwater for growth will gradually appear on a large space and time scale. This research has determined that WUE has the strongest memory effect, but the weakest sensitivity (Figs. S6c and S8c), and that regional WUE growth shows a significant time lag (Fig. 6). Another study has shown that in all biological communities from grassland to forest, the entire ecosystem has an inherent system sensitivity to water availability, regardless of hydrological and climatic conditions, or in other words, WUE has a strong memory effect (Campos et al., 2013). This suggests that the rules for managing and organizing species in arid ecosystems according to their tolerance to hydrologic stress are robust despite the long-term disturbance of low rainfall (Campos et al., 2013).

The growth of desert riparian vegetation requires moderate water conditions. When an ecosystem is mainly constrained by water resources, if drought continues, the resilience of the ecosystem may collapse as the ecosystem WUE decreases to a certain threshold (Campos et al., 2013). Crossing this threshold will lead to reorganization of the biological community (Campos et al., 2013). However, some wet areas characterized by peatlands, bogs, and wetlands experience water surplus (Jiao et al., 2021), and it has been reported that waterlogging limits productivity in these areas (Minasny et al., 2019). Therefore, increasing the amount of water resources does not necessarily make an ecosystem more favorable to vegetation production and efficient use of water. According to the theory of moderate interference, under moderate water delivery conditions, a combination of grasses and shrubs will form (Ling et al., 2019) where the overall biomass level of the basin is relatively high and water use efficiency is also high. Currently, ecosystem water use has not been widely used to restrict GPP on a regional or global scale. Specifically, one study showed that terrestrial carbon absorption does not increase proportionately with an increase in water consumption (i.e., evapotranspiration), but is largely (about 90%) driven by increasing water use efficiency (Cheng et al., 2017). This provides us with a direction for thought and strong support to explore the optimal relationship between GPP and WUE. In this regard, the following research question can be proposed: what level of watershed biomass can be restored to maximize the benefits of water conservation during ecological water transport? By calculating the multi-year average GPP and WUE for each pixel, a strong correlation between GPP and WUE was found ($R^2 = 0.925$; $p < 0.05$). Therefore, a polynomial function relationship was established between WUE and GPP, and the WUE threshold corresponding to the GPP threshold was estimated (Fig. 9). For the Tarim River Basin, when the GPP and WUE are 216.44 $g\,C\,m^{-2}$ and 0.93 $g\,C\,m^{-2}\,mm^{-1}$ respectively, the optimal combination of ecological and water transport benefits can be achieved. The underlying reason for the disproportionate changes in WUE and GPP is that excessive water transport leads to shallow groundwater depth, which leads to increased soil salinization and excessive water content (Ling et al., 2020). Excessive water means that plant roots may be anaerobic or anoxic for a long time, which will limit the energy production required for plant respiration and vegetation growth (Si et al., 2015). In addition, the high salt content of the soil means that excess water accelerates accumulation of sodium and chloride ions in the root system (Si et al., 2015), which in turn damages the function of plant roots and destroys the normal physiological process of *P. euphratica* roots (Si et al., 2015). Therefore, GPP and WUE threshold points should be taken as the basis for ecological water release regulation to achieve double optimization of GPP and WUE when carrying out ecological restoration in the watershed. Ecological restoration is not endless. Finding such a threshold point can provide an important reference for long-term and rational water resource management in water-scarce inland river basins, and can also provide an important target for promoting stable and sustainable development of the region.

5. Conclusions

In this study, a novel multi-model fusion framework was constructed, including two modules: the first using an ensemble function that integrates a logistic function and an asymmetric Gaussian function to automatically identify the change characteristics of ecological indicators; and the second, based on an ARI multiple regression analysis model and the sensitivity index, to reveal the response mechanism of ecological indicators to changes in their environment. This framework can not only identify the nonlinear change process of ecological indicators, but also detect non-monotonic change processes in which ecological indicators undergo degradation after restoration or the reverse. Moreover, future development trends can be predicted according to the recent shape of ecological indicator change curves. Research and application have demonstrated that this framework can accurately detect major disturbances in the long-term evolution of ecological indicators (especially GPP). In addition, quantifying the sensitivity and memory effect of ecological indicators to changes in their environment can further reveal the driving mechanism of ecological indicator change patterns. Therefore, this study used this framework, combined with multi-source remote sensing and groundwater depth monitoring data, to carry out a comprehensive analysis of the long-term evolution law, future development trend, and driving mechanism of desert riparian forest ecological indicators under environmental changes. The results of this study also have important guiding significance for future rational and effective water-management activities in other inland river basins in arid areas.

Under the influence of enhanced water resource management activities, the GPP in the Tarim River Basin generally shows an increasing trend and is expected to continue to rise or to maintain a high-level stable state. To carry out accurate ecological water supply forecasting and realize efficient utilization of ecological water according to the eight change patterns presented by GPP, the regions with logistic and logarithmic growth patterns were regarded as high-level stable regions, where protection was given priority to maintain the stability of the

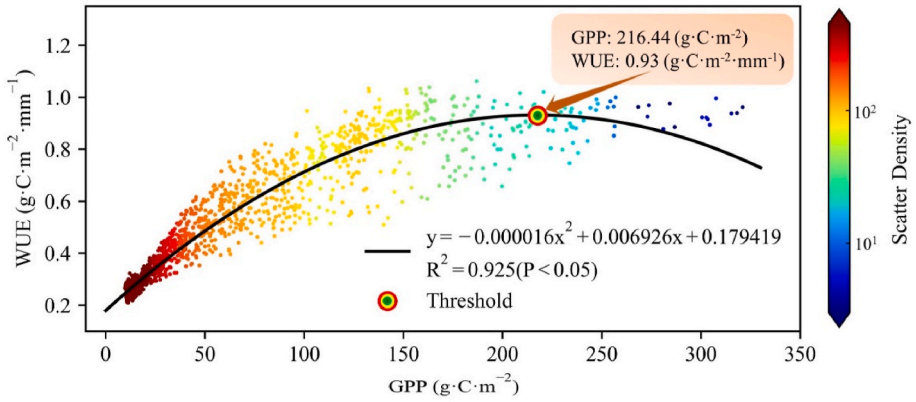

Fig. 9. The polynomial function relationship of WUE with GPP.

ecosystem. Areas showing other change patterns were all treated as key control areas, where restoration efforts should be strengthened to promote their recovery. In the process of ecological management, persistence is essential. The longest duration of GPP change was 15 years, and therefore, in the process of ecological restoration in desert riparian forest, it is necessary to achieve long-term, continuous, and accurate water volume regulation. Moreover, the years of GPP changeover coincided with the implementation years of major water resource reform initiatives in the Tarim River Basin (1990, 2001, and 2011), which verifies the accuracy of the research framework.

WUE in arid areas has a maximum threshold with increasing GPP, which provides an important basis for ecological water supply. Excessive water transfer inhibits biomass growth and leads to low water use efficiency; moderate water transfer is conducive to vegetation production and makes efficient use of ecological water. It was found that when GPP reached 216.44 $g\,C\,m^{-2}$, the highest WUE was attained, at 0.93 $g\,C\,m^{-2}\,mm^{-1}$. The threshold point should be taken as the goal of ecological restoration to realize dual optimization of ecological and water resource benefits when conducting ecological water supply management.

Arid ecosystems are inherently sensitive to water availability (the memory effect) and will have a delayed response to water use when faced with external disturbances. In 80.60% of pixels, GPP showed a weak memory effect ($\alpha < 0.4$), but in 53.73% of pixels, WUE showed a strong memory effect ($\alpha > 0.4$). This means that changes in WUE on the regional scale showed a significant time lag. Among the three ecological indicators, GPP was the most sensitive to environmental change and LAI, and the correlation between GPP and LAI was also the strongest ($p < 0.001$). LAI can therefore be used as the main factor for judging plant growth.

Author contribution

Z.K. obtained, processed, and analyzed the data, drew charts and completed the original manuscript. F.H. and H.L. designed the research and methodology. F.H. wrote the program code, drew the chart, and modified the content of the method part. H.L. completed an in-depth discussion of the results of the study and revised the draft. M.D. contributed to the results discussion section. M.L and J.Y contributed to the processing and analysis of saturated vapor pressure deficit and groundwater data. All the authors reviewed and approved the final manuscript.

Declaration of competing interest

The authors declare that they have no known competing financial interests or personal relationships that could have appeared to influence the work reported in this paper.

Acknowledgements

This research was funded by the Xinjiang Tianshan Youth Program (2019Q006), the West Light Foundation of Chinese Academy of Sciences (2019-XBQNXZ-A-001), and the Xinjiang Water Conservancy Science and Technology Special Fund Project (XSKJ-2022-10).

Appendix A. Supplementary data

Supplementary data to this article can be found online at https://doi.org/10.1016/j.jenvman.2022.115592.

References

Ahlstrom, A., Raupach, M.R., Schurgers, G., Smith, B., Arneth, A., Jung, M., Reichstein, M., Canadell, J.G., Friedlingstein, P., Jain, A.K., Kato, E., Poulter, B., Sitch, S., Stocker, B.D., Viovy, N., Wang, Y.P., Wiltshire, A., Zaehle, S., Zeng, N., 2015. The dominant role of semi-arid ecosystems in the trend and variability of the land CO2 sink. Science 348 (6237), 895–899.

Beer, C., Reichstein, M., Tomelleri, E., Ciais, P., Jung, M., Carvalhais, N., Rodenbeck, C., Arain, M.A., Baldocchi, D.D., Bonan, G.B., Bondeau, A., Cescatti, A., Lasslop, G., Lindroth, A., Lomas, M., Luyssaert, S., Margolis, H., Oleson, K.W., Roupsard, O., Veenendaal, E., Viovy, N., Williams, C., Woodward, F.I., Papale, D., 2010. Terrestrial gross carbon dioxide uptake: global distribution and covariation with climate. Science 329 (5993), 834–838.

Campos, G.E.P., Moran, M.S., Huete, A., Zhang, Y., Bresloff, C., Huxman, T.E., Eamus, D., Bosch, D.D., Buda, A.R., Gunter, S.A., Scalley, T.H., Kitchen, S.G., McClaran, M.P., McNab, W.H., Montoya, D.S., Morgan, J.A., Peters, D.P.C., Sadler, E.J., Seyfried, M. S., Starks, P.J., 2013. Ecosystem resilience despite large-scale altered hydroclimatic conditions. Nature 494 (7437), 349–352.

Cao, R., Chen, J., Shen, M., Tang, Y., 2015. An improved logistic method for detecting spring vegetation phenology in grasslands from MODIS EVI time-series data. Agric. For. Meteorol. 200, 9–20.

Che, M., Chen, B., Innes, J.L., Wang, G., Dou, X., Zhou, T., Zhang, H., Yan, J., Xu, G., Zhao, H., 2014. Spatial and temporal variations in the end date of the vegetation growing season throughout the Qinghai-Tibetan Plateau from 1982 to 2011. Agric. For. Meteorol. 189, 81–90.

Chen, J.M., Ju, W., Ciais, P., Viovy, N., Liu, R., Liu, Y., Lu, X., 2019. Vegetation structural change since 1981 significantly enhanced the terrestrial carbon sink. Nat. Commun. 10, 4259.

Chen, X., Maignan, F., Viovy, N., Bastos, A., Goll, D., Wu, J., Liu, L., Yue, C., Peng, S., Yuan, W., da Conceicao, A.C., O'Sullivan, M., Ciais, P., 2020. Novel representation of leaf phenology improves simulation of amazonian evergreen forest photosynthesis in a land surface model. J. Adv. Model. Earth Syst. 12 (1).

Cheng, L., Zhang, L., Wang, Y.P., Canadell, J.G., Chiew, F.H.S., Beringer, J., Li, L., Miralles, D.G., Piao, S., Zhang, Y., 2017. Recent increases in terrestrial carbon uptake at little cost to the water cycle. Nat. Commun. 8, 110.

Chu, J., Syktus, J., McAlpine, C., Thatcher, M., Scarth, P., Jeffrey, S., Katzfey, J., Zhang, H., McGregor, J., Adams-Hosking, C., 2011. Validation of land surface products for modelling the climate impacts of large-scale revegetation in Queensland. In: MODSIM 2011 - 19th International Congress on Modelling and Simulation – Sustaining Our Future: Understanding and Living with Uncertainty, pp. 2676–2682. December 2011.

Crouzeilles, R., Curran, M., Ferreira, M.S., Lindenmayer, D.B., Grelle, C.E.V., Rey Benayas, J.M., 2016. A global meta-analysis on the ecological drivers of forest restoration success. Nat. Commun. 7, 11666.

Dai, L., Vorselen, D., Korolev, K.S., Gore, J., 2012. Generic indicators for loss of resilience before a tipping point leading to population collapse. Science 336 (6085), 1175–1177.

de Jong, R., Verbesselt, J., Schaepman, M.E., de Bruin, S., 2012. Trend changes in global greening and browning: contribution of short-term trends to longer-term change. Global Change Biol. 18 (2), 642–655.
Deng, M., Huang, Q., Chang, J., Huang, S., 2020. Large-scale ecological operation research and practice. J. Hydraul. Eng. 51 (7), 757–773.
Deng, M., Yang, P., Zhou, H., Xu, H., 2017. Water conversion and strategy of ecological water conveyance in the lower reaches of the Tarim River. Arid Zone Res. 34, 717–726.
Fang, X., Zhu, Q., Ren, L., Chen, H., Wang, K., Peng, C., 2018. Large-scale detection of vegetation dynamics and their potential drivers using MODIS images and BFAST: a case study in Quebec, Canada. Remote Sens. Environ. 206, 391–402.
Fensholt, R., Langanke, T., Rasmussen, K., Reenberg, A., Prince, S.D., Tucker, C., Scholes, R.J., Le, Q.B., Bondeau, A., Eastman, R., Epstein, H., Gaughan, A.E., Hellden, U., Mbow, C., Olsson, L., Paruelo, J., Schweitzer, C., Seaquist, J., Wessels, K., 2012. Greenness in semi-arid areas across the globe 1981-2007 - an Earth Observing Satellite based analysis of trends and drivers. Remote Sens. Environ. 121, 144–158.
Friedlingstein, P., O'Sullivan, M., Jones, M.W., Andrew, R.M., Hauck, J., Olsen, A., Peters, G.P., Peters, W., Pongratz, J., Sitch, S., Quere, C.L., Canadell, J.G., Ciais, P., Jackson, R.B., Alin, S., Aragao, L.E.O.C., Arneth, A., Arora, V., Bates, N.R., Becker, M., Benoit-Cattin, A., Bittig, H.C., Bopp, L., Bultan, S., Chandra, N., Chevallier, F., Chini, L.P., Evans, W., Florentie, L., Forster, P.M., Gasser, T., Gehlen, M., Gilfillan, D., Gkritzalis, T., Gregor, L., Gruber, N., Harris, I., Hartung, K., Haverd, V., Houghton, R.A., Ilyina, T., Jain, A.K., Joetzjer, E., Kadono, K., Kato, E., Kitidis, V., Korsbakken, J.I., Landschutzer, P., Lefevre, N., Lenton, A., Lienert, S., Liu, Z., Lombardozzi, D., Marland, G., Metzl, N., Munro, D.R., Nabel, J.E.M.S., Nakaoka, S.I., Niwa, Y., OBrien, K., Ono, T., Palmer, P.I., Pierrot, D., Poulter, B., Resplandy, L., Robertson, E., Rodenbeck, C., Schwinger, J., Seferian, R., Skjelvan, I., Smith, A.J.P., Sutton, A.J., Tanhua, T., Tans, P.P., Tian, H., Tilbrook, B., van der Werf, G., Vuichard, N., Walker, A.P., Wanninkhof, R., Watson, A.J., Willis, D., Wiltshire, A.J., Yuan, W., Yue, X., Zaehle, S., 2020. Global carbon budget 2020. Earth Syst. Sci. Data 12 (4), 3269–3340.
Hu, S., Ma, R., Sun, Z., Ge, M., Zeng, L., Huang, F., Bu, J., Wang, Z., 2021. Determination of the optimal ecological water conveyance volume for vegetation restoration in an arid inland river basin, northwestern China. Sci. Total Environ. 788, 147775.
Ichii, K., Kondo, M., Okabe, Y., Ueyama, M., Kobayashi, H., Lee, S.J., Saigusa, N., Zhu, Z., Myneni, R.B., 2013. Recent changes in terrestrial gross primary productivity in Asia from 1982 to 2011. Rem. Sens. 5 (11), 6043–6062.
Jamali, S., Jonsson, P., Eklundh, L., Ardo, J., Seaquist, J., 2015. Detecting changes in vegetation trends using time series segmentation. Remote Sens. Environ. 156, 182–195.
Jasechko, S., Sharp, Z.D., Gibson, J.J., Birks, S.J., Yi, Y., Fawcett, P.J., 2013. Terrestrial water fluxes dominated by transpiration. Nature 496 (7445), 347–351.
Jiang, C.Y., Ryu, Y., Fang, H.L., Myneni, R., Claverie, M., Zhu, Z.C., 2017. Inconsistencies of interannual variability and trends in long-term satellite leaf area index products. Global Change Biol. 23 (10), 4133–4146.
Jiao, W., Wang, L., Smith, W.K., Chang, Q., Wang, H., D'Odorico, P., 2021. Observed increasing water constraint on vegetation growth over the last three decades. Nat. Commun. 12 (1), 3777.
Jonsson, P., Eklundh, L., 2002. Seasonality extraction by function fitting to time-series of satellite sensor data. IEEE Trans. Geosci. Rem. Sens. 40 (8), 1824–1832.
Keenan, T.F., Hollinger, D.Y., Bohrer, G., Dragoni, D., Munger, J.W., Schmid, H.P., Richardson, A.D., 2013. Increase in forest water-use efficiency as atmospheric carbon dioxide concentrations rise. Nature 499 (7458), 324–327.
Knapp, A.K., Smith, M.D., 2001. Variation among biomes in temporal dynamics of aboveground primary production. Science 291 (5503), 481–484.
Kochendorfer, J., Castillo, E.G., Haas, E., Oechel, W.C., Paw, K.T.U., 2011. Net ecosystem exchange, evapotranspiration and canopy conductance in a riparian forest. Agric. For. Meteorol. 151 (5), 544–553.
Li, D., Wu, S., Liu, L., Zhang, Y., Li, S., 2018. Vulnerability of the global terrestrial ecosystems to climate change. Global Change Biol. 24 (9), 4095–4106.
Ling, H., Guo, B., Yan, J., Deng, X., Xu, H., Zhang, G., 2020. Enhancing the positive effects of ecological water conservancy engineering on desert riparian forest growth in an arid basin. Ecol. Indicat. 118, 106797.
Ling, H., Xu, H., Guo, B., Deng, X., Zhang, P., Wang, X., 2019. Regulating water disturbance for mitigating drought stress to conserve and restore a desert riparian forest ecosystem. J. Hydrol. 572, 659–670.
Ling, H., Zhang, P., Xu, H., Zhang, G., 2016. Determining the ecological water allocation in a hyper-arid catchment with increasing competition for water resources. Global Planet. Change 145, 143–152.
Liu, B., Guan, H., Zhao, W., Yang, Y., Li, S., 2017. Groundwater facilitated water-use efficiency along a gradient of groundwater depth in arid northwestern China. Agric. For. Meteorol. 233, 235–241.
Liu, J., Zang, C., Tian, S., Liu, J., Yang, H., Jia, S., You, L., Liu, B., Zhang, M., 2013. Water conservancy projects in China: achievements, challenges and way forward. Glob. Environ. Change Hum. Policy Dimens. 23 (3), 633–643.
Liu, X., Feng, X., Fu, B., 2020. Changes in global terrestrial ecosystem water use efficiency are closely related to soil moisture. Sci. Total Environ. 698, 134165.
Liu, Y.B., Xiao, J.F., Ju, W.M., Zhu, G.L., Wu, X.C., Fan, W.L., Li, D.Q., Zhou, Y.L., 2018. Satellite-derived LAI products exhibit large discrepancies and can lead to substantial uncertainty in simulated carbon and water fluxes. Remote Sens. Environ. 206, 174–188.
Ma, J., Xiao, X., Miao, R., Li, Y., Chen, B., Zhang, Y., Zhao, B., 2019. Trends and controls of terrestrial gross primary productivity of China during 2000-2016. Environ. Res. Lett. 14 (8), 084032.
Madani, N., Kimball, J.S., Parazoo, N.C., Ballantyne, A.P., Tagesson, T., Jones, L.A., Reichle, R.H., Palmer, P.I., Velicogna, I., Bloom, A.A., Saatchi, S., Liu, Z., Geruo, A., 2020. Below-surface water mediates the response of African forests to reduced rainfall. Environ. Res. Lett. 15 (3), 034063.
Martin, T.G., Watson, J.E.M., 2016. Intact ecosystems provide best defence against climate change. Nat. Clim. Change 6 (2), 122–124.
Minasny, B., Berglund, O., Connolly, J., Hedley, C., de Vries, F., Gimona, A., Kempen, B., Kidd, D., Lilja, H., Malone, B., McBratney, A., Roudier, P., O'Rourke, S., Rudiyanto Padarian, J., Poggio, L., ten Caten, A., Thompson, D., Tuve, C., Widyatmanti, W., 2019. Digital mapping of peatlands-A critical review. Earth Sci. Rev. 196, 102870.
Piao, S., Wang, X., Park, T., Chen, C., Lian, X., He, Y., Bjerke, J.W., Chen, A., Ciais, P., Tommervik, H., Nemani, R.R., Myneni, R.B., 2020. Characteristics, drivers and feedbacks of global greening. Nat. Rev. Earth Environ. 1 (1), 14–27.
Poulter, B., Frank, D., Ciais, P., Myneni, R.B., Andela, N., Bi, J., Broquet, G., Canadell, J. G., Chevallier, F., Liu, Y.Y., Running, S.W., Sitch, S., van der Werf, G.R., 2014. Contribution of semi-arid ecosystems to interannual variability of the global carbon cycle. Nature 509 (7502), 600–603.
Ryu, Y., Berry, J.A., Baldocchi, D.D., 2019. What is global photosynthesis? History, uncertainties and opportunities. Remote Sens. Environ. 223, 95–114.
Scott, R.L., Huxman, T.E., Williams, D.G., Goodrich, D.C., 2006. Ecohydrological impacts of woody-plant encroachment: seasonal patterns of water and carbon dioxide exchange within a semiarid riparian environment. Global Change Biol. 12 (2), 311–324.
Seddon, A.W.R., Macias-Fauria, M., Long, P.R., Benz, D., Willis, K.J., 2016. Sensitivity of global terrestrial ecosystems to climate variability. Nature 531 (7593), 229–232.
Si, J., Feng, Q., Yu, T., Zhao, C., Li, W., 2015. Variation in Populus euphratica foliar carbon isotope composition and osmotic solute for different groundwater depths in an arid region of China. Environ. Monit. Assess. 187 (11), 705.
Song, X.P., Sexton, J.O., Huang, C., Channan, S., Townshend, J.R., 2016. Characterizing the magnitude, timing and duration of urban growth from time series of Landsat-based estimates of impervious cover. Remote Sens. Environ. 175, 1–13.
Su, Y., Li, X., Feng, M., Nian, Y., Huang, L., Xie, T., Zhang, K., Chen, F., Huang, W., Chen, J., Chen, F., 2021. High agricultural water consumption led to the continued shrinkage of the Aral Sea during 1992-2015. Sci. Total Environ. 777, 145993.
Sun, Y., Piao, S., Huang, M., Ciais, P., Zeng, Z., Cheng, L., Li, X., Zhang, X., Mao, J., Peng, S., Poulter, B., Shi, X., Wang, X., Wang, Y., Zeng, H., 2016. Global patterns and climate drivers of water-use efficiency in terrestrial ecosystems deduced from satellite-based datasets and carbon cycle models. Global Ecol. Biogeogr. 25 (3), 311–323.
Tagesson, T., Tian, F., Schurgers, G., Horion, S., Scholes, R., Ahlstrom, A., Ardo, J., Moreno, A., Madani, N., Olin, S., Fensholt, R., 2021. A physiology-based Earth observation model indicates stagnation in the global gross primary production during recent decades. Global Change Biol. 27 (4), 836–854.
Tong, X., Brandt, M., Yue, Y., Horion, S., Wang, K., De Keersmaecker, W., Tian, F., Schurgers, G., Xiao, X., Luo, Y., Chen, C., Myneni, R., Shi, Z., Chen, H., Fensholt, R., 2018. Increased vegetation growth and carbon stock in China karst via ecological engineering. Nat. Sustain. 1 (1), 44–50.
van der Meijden, C.M., Veringa, H.J., Rabou, L.P.L.M., 2010. The production of synthetic natural gas (SNG): a comparison of three wood gasification systems for energy balance and overall efficiency. Biomass Bioenergy 34 (3), 302–311.
Verbesselt, J., Hyndman, R., Newnham, G., Culvenor, D., 2010. Detecting trend and seasonal changes in satellite image time series. Remote Sens. Environ. 114 (1), 106–115.
Wang, C., Jiang, Q.o., Shao, Y., Sun, S., Xiao, L., Guo, J., 2019. Ecological environment assessment based on land use simulation: a case study in the Heihe River Basin. Sci. Total Environ. 697, 133928.
Wessels, K.J., van den Bergh, F., Scholes, R.J., 2012. Limits to detectability of land degradation by trend analysis of vegetation index data. Remote Sens. Environ. 125, 10–22.
Xiao, Z., Liang, S., Wang, J., Jiang, B., Li, X., 2011. Real-time retrieval of Leaf Area Index from MODIS time series data. Remote Sens. Environ. 115 (1), 97–106.
Xiao, Z., Liang, S., Wang, J., Xiang, Y., Zhao, X., Song, J., 2016. Long-time-series global land surface satellite leaf area index product derived from MODIS and AVHRR surface reflectance. IEEE Trans. Geosci. Rem. Sens. 54 (9), 5301–5318.
Yang, Y., Guan, H., Batelaan, O., McVicar, T.R., Long, D., Piao, S., Liang, W., Liu, B., Jin, Z., Simmons, C.T., 2016. Contrasting responses of water use efficiency to drought across global terrestrial ecosystems. Sci. Rep. 6, 23284.
Yao, J., Liu, H., Huang, J., Gao, Z., Wang, G., Li, D., Yu, H., Chen, X., 2020. Accelerated dryland expansion regulates future variability in dryland gross primary production. Nat. Commun. 11 (1), 1665.
Yao, Y., Liang, S., Li, X., Chen, J., Wang, K., Jia, K., Cheng, J., Jiang, B., Fisher, J.B., Mu, Q., Gruenwald, T., Bernhofer, C., Roupsard, O., 2015. A satellite-based hybrid algorithm to determine the Priestley-Taylor parameter for global terrestrial latent heat flux estimation across multiple biomes. Remote Sens. Environ. 165, 216–233.
Yu, G., Song, X., Wang, Q., Liu, Y., Guan, D., Yan, J., Sun, X., Zhang, L., Wen, X., 2008. Water-use efficiency of forest ecosystems in eastern China and its relations to climatic variables. New Phytol. 177 (4), 927–937.
Yuan, W., Zheng, Y., Piao, S., Ciais, P., Lombardozzi, D., Wang, Y., Ryu, Y., Chen, G., Dong, W., Hu, Z., Jain, A.K., Jiang, C., Kato, E., Li, S., Lienert, S., Liu, S., Nabel, J.E. M.S., Qin, Z., Quine, T., Sitch, S., Smith, W.K., Wang, F., Wu, C., Xiao, Z., Yang, S., 2019. Increased atmospheric vapor pressure deficit reduces global vegetation growth. Sci. Adv. 5 (8), eaax1396.

Zhang, L., Xiao, J., Zheng, Y., Li, S., Zhou, Y., 2020. Increased carbon uptake and water use efficiency in global semi-arid ecosystems. Environ. Res. Lett. 15 (3), 034022.
Zhang, X.Y., Friedl, M.A., Schaaf, C.B., Strahler, A.H., Hodges, J.C.F., Gao, F., Gao, F., Reed, B.C., Huete, A., 2003. Monitoring vegetation phenology using MODIS. Remote Sens. Environ. 84 (3), 471–475.
Zhao, J., Feng, H., Xu, T., Xiao, J., Guerrieri, R., Liu, S., Wu, X., He, X., He, X., 2021. Physiological and environmental control on ecosystem water use efficiency in response to drought across the northern hemisphere. Sci. Total Environ. 758, 143599.